



## **Air quality deterioration episode associated with typhoon over the complex topographic environment in central Taiwan**

**Chuan-Yao Lin\*, Yang-Fan Sheng, Wan-Chin Chen, Charles, C. K. Chou, Yi-**

**Yun Chien, Wen-Mei Chen**

Research Center for Environmental Changes, Academia Sinica, Taipei, Taiwan.

\*Corresponding author

**Chuan Yao Lin,**

Research Center for Environmental Changes, Academia Sinica, Taipei, Taiwan

128 Sec. 2, Academia Rd, Nankang, Taipei 115, Taiwan

(E-mail: [yao435@rceec.sinica.edu.tw](mailto:yao435@rceec.sinica.edu.tw), Tel.: +886-2-27875892, Fax: +886-2-27833584),



1 **Abstract:**

2 Air pollution is typically at its lowest in Taiwan during summer. The mean  
3 concentrations of PM<sub>10</sub>, PM<sub>2.5</sub>, and daytime ozone (08:00–17:00 LST) during summer  
4 (June–August) over central Taiwan are 35–40 µg/m<sup>3</sup>, 18–22 µg/m<sup>3</sup>, and 30–42 ppb,  
5 respectively, between 2004 and 2019. Sampling analysis revealed that the contribution  
6 of organic carbon (OC) in PM<sub>2.5</sub> could exceed 30% in urban and inland mountain sites  
7 during July in 2017 and 2018. Frequent episodes of air quality deterioration occur over  
8 the western plains of Taiwan when an easterly typhoon circulation interacts with the  
9 complex topographic structure of the island. We explored an episode of air quality  
10 deterioration that was associated with a typhoon between 15 and 17 July 2018, using the  
11 Weather Research Forecasting with Chemistry (WRF-Chem) model. The results  
12 indicated that the continual formation of low-pressure systems or typhoons in the area  
13 between Taiwan and Luzon island in the Philippines provided a strong easterly ambient  
14 flow, which lasted for an extended period between 15 and 17 July. The interaction  
15 between the easterly flow and Taiwan’s Central Mountain Range (CMR) resulted in  
16 stable weather conditions and weak wind speed in western Taiwan during the study  
17 period. Numerical modeling also indicated that a lee side vortex easily formation and  
18 the wind direction could be changed from southwesterly to northwesterly over central  
19 Taiwan because of the interaction between the typhoon circulation and the CMR. The



20 northwesterly wind coupled with a sea breeze was conducive to the transport of air  
21 pollutants, from the coastal upstream industrial and urban areas to the inland area. The  
22 dynamic process for the wind direction changed given a reasonable explanation why the  
23 observed  $\text{SO}_4^{2-}$  became the major contributor to  $\text{PM}_{2.5}$  during the episode.  $\text{SO}_4^{2-}$   
24 contribution proportions (%) to  $\text{PM}_{2.5}$  at the coastal, urban, and mountain sites were 9.4  
25  $\mu\text{g}/\text{m}^3$  (30.5%), 12.1  $\mu\text{g}/\text{m}^3$  (29.9%), and 11.6  $\mu\text{g}/\text{m}^3$  (29.7%), respectively. Moreover,  
26 the variation of the boundary layer height had a strong effect on the concentration level  
27 of both  $\text{PM}_{2.5}$  and ozone. The combination of the lee vortex and land-sea breeze, as well  
28 as the boundary layer development, were the key mechanisms in air pollutants  
29 accumulation and transport. As typhoons frequently occur around Taiwan during  
30 summer and fall, and their effect on the island's air quality merits further research  
31 attention.

32

33

34

35

36

37

38



39 **1. Introduction:**

40 Tropical cyclones (also known as typhoons) are a frequent occurrence in East Asia  
41 during summer and fall. Typhoons significantly affect not only meteorological parameters  
42 but also air quality. That is because air pollution is strongly related to atmospheric  
43 conditions, and typhoon circulation typically alters atmospheric stability and air pollutant  
44 diffusion in specific locations. For example, researchers revealed that ozone episodes in  
45 Hong Kong and southeastern China are strongly related to the passage of typhoons as  
46 they approach the area (Lee et al., 2002; Ding et al., 2004; Huang et al., 2005 and 2006;  
47 Yang et al., 2012; Zhang et al., 2013; Zhang et al., 2014; Wei et al., 2016; Yan et al. 2016;  
48 Luo et al. 2018; Deng et al. 2019; Hung et al., 2021). The stagnant meteorological  
49 conditions associated with strong subsidence and stable stratification in the boundary  
50 layer results in pollutant accumulation before typhoons make landfall. Huang et al. (2005)  
51 reported that approximately 30% of total ozone in Hong Kong was due to local chemical  
52 production in the lower atmospheric boundary layer, and approximately 70% was  
53 contributed by long-range transport from southern China (i.e., the Pearl River Delta).  
54 According to the dynamic process perspective, Chow et al. (2018) reported frequent high-  
55 O<sub>3</sub> days when typhoons were located between Hong Kong and Taiwan (Fig. 1a) due to  
56 the influence of the typhoon position and associated atmospheric circulations on air  
57 quality.



58 Taiwan also experiences air quality deterioration as typhoons approach (Feng et al.  
59 2007; Chang et al., 2011, Cheng et al., 2014; Hsu and Cheng, 2019). However, not all  
60 typhoons are associated with poorer air quality in Taiwan. The effect of typhoons on air  
61 quality is highly related to the location of the typhoon and its circulation's interaction  
62 with Taiwan's Central Mountain Range (CMR; Fig. 1b). Thus, the mechanism of the  
63 formation of poor air quality may differ between Taiwan and Hong Kong. Air quality  
64 deterioration frequently occurs over the western plains of Taiwan when typhoons pass  
65 between Taiwan and Luzon island in the Philippines; the distance of the typhoons from  
66 Taiwan is typically several hundred kilometers but may even be greater than 1000  
67 kilometers. Under such conditions, the weather is typically stable, with clear skies, strong  
68 solar intensity, and weak wind speeds over Taiwan's western plains because of the  
69 interactions of the typhoon's easterly circulations with the CMR. Furthermore, such  
70 typhoons are usually associated with a Pacific high-pressure system during summer; thus,  
71 the air temperature may be high. For example, researchers have noted that typhoon's  
72 secondary circulation may enhance subsidence and result in a heat wave, clear skies, and  
73 weak wind speed over Taiwan or Southern China (e.g., Ding et al. 2004; Huang et al. 2005;  
74 Jiang et al., 2015; Shu et al. 2016; Lam, et al., 2018) and thus adversely affect air quality  
75 as well. In Taiwan, this phenomenon is particularly attributed to the blocking effect of the  
76 CMR. The CMR occupies approximately two-thirds of Taiwan's landmass (300 km × 100



77 km) and lies NNE–SSW (Fig. 1b), with an average terrain height of approximately 2000  
78 m (Lin and Chen, 2002; Lin et al., 2011) and some peaks of nearly 4000 m. The CMR  
79 has a major effect on local circulation and interferes with the prevailing winds. When a  
80 typhoon is located between Taiwan and Luzon, the low-level easterly airflow easily splits  
81 northern and southern Taiwan and moves around the island, forming a vortex at the lee  
82 side of the mountain (Hunt and Synder, 1980; Smolarkiewicz and Rotunno, 1989; Lin,  
83 Y.L. 1993; Lin et al. 2007). On the leeside of the CMR, wind speeds are weak (Lin et al.,  
84 2007) and the atmospheric conditions are more stable than on the windward side of  
85 eastern Taiwan. Under these favorable conditions, air pollutants readily accumulate and  
86 result in high ozone and aerosol concentrations over western Taiwan.

87 Summer and fall are regarded as “typhoon season” over Taiwan and throughout  
88 East Asia. Statistically, more than 20 typhoons form in the western Pacific Ocean per year,  
89 and approximately 3–4 typhoons directly strike Taiwan (Lin et al. 2011; Tu and Chen  
90 2019). Records from Taiwan’s Central Weather Bureau (CWB) indicate that 18% of  
91 typhoons (Type 5; <https://www.cwb.gov.tw/V8/C/K/Encyclopedia/typhoon/typhoon.pdf>)  
92 between 1911 and 2019 did not make landfall but passed between Taiwan and Luzon. The  
93 wind circulations of this type of typhoon were easterly or southeasterly depending on the  
94 location of the typhoons. Thus, it is not uncommon for more than 10 typhoons per year  
95 to pass near Taiwan and affect the island’s air quality. The impact of the interaction



96 between the typhoon's circulation and the CMR on the air quality on the lee side of the  
97 mountain is more serious than in other areas.

98 To date, air pollution episodes with a formation mechanism associated with the  
99 interactions between typhoon circulation and the CMR have not been thoroughly  
100 documented in Taiwan. In this study, we investigated a major air quality event that  
101 occurred on 17 July 2018, with a maximum O<sub>3</sub> concentration of 134 ppb and the daily  
102 maximum aerosol concentration for PM<sub>10</sub> (PM<sub>2.5</sub>) reaching 152 μg/m<sup>3</sup> (70 μg/m<sup>3</sup>) in  
103 inland rural areas of central Taiwan. We used the Weather Research Forecasting with  
104 Chemistry model (WRF-Chem, version 3.9; Grell et al., 2005) to study the processes and  
105 mechanisms of formation of the air pollution episode. The remainder of this paper is  
106 organized as follows: Sect. 2 describes the data sources and sampling measurement during  
107 the study period; Sect. 3 presents the model and settings used in this study; Sect. 4  
108 presents the air quality characteristics and measurements recorded over the western plains  
109 of Taiwan; Sect. 5 describes and discusses the simulation results of air quality associated  
110 with the typhoon event using WRF-Chem; and finally, Sect. 6 provides the conclusions.

111

## 112 **2. Data sources and measurement**

113 We collected measurements of hourly PM<sub>10</sub>, PM<sub>2.5</sub>, and other pollutants (O<sub>3</sub>, NO<sub>x</sub>,  
114 CO, and SO<sub>2</sub>) as well as meteorological parameters (air temperature, wind field, and  
115 rainfall) from Taiwan Environmental Protection Administration (TEPA) air quality



116 monitoring stations. To elucidate the spatial distribution of air pollutants, we classified  
117 the observed stations over central Taiwan into “coast,” “urban,” and “mountain.” Each  
118 of these categories represents the mean concentration of the numbers derived from  
119 stations of the same type. The coast category included two stations: Shalu (SL) and  
120 Xianxi (XX; Fig. 1c). The urban category included five stations: Fengyuan (FY), Xitun  
121 (XT), Zhongming (ZM), Changhua (CH), and Dali (DL; Fig. 1c). The mountain  
122 category included three stations: Nantou (NT), Zhushan (ZS), and Puli (PL), which  
123 were located nearby or in basins surrounded by high mountains (Fig. 1c). Two stations  
124 on small islands were also considered in the analysis. One was in Kinmen (KM), which  
125 is located close to Xiamen city in southeast China, and the other was Magong (MG)  
126 station located in the Taiwan Strait (Fig. 1a).

127 To explore the air pollution episodes during summer, we recorded data in central  
128 Taiwan in July 2017 and 2018. For the summer campaigns, we employed three  
129 sampling sites (the squares in Fig. 1c), Shalu (SL, 24.23 °N, 120.57 °E; the same  
130 location as the TEPA station), Zhushan (ZS, 23.76 °N, 120.68 °E; the same location as  
131 the TEPA station), and Chung Shan Medical University (CSM) (24.12 °N, 120.65 °E;  
132 Fig. 1c). ZS is a suburban site located in a complex valley surrounded by hills (300–  
133 500 m) and high mountains (CMR; elevation > 2000 m) to the east and south,  
134 respectively. The remaining two sampling sites, SL and CSM, were located in a coastal  
135 suburban and urban area (Fig. 1c), respectively. The sampling period of each sample  
136 was 12 h; daytime samples were collected from 08:00 to 19:00 LST, whereas nighttime  
137 sampling was conducted from 20:00 LST to 07:00 LST. We determined mass  
138 concentrations of the aerosols using a gravimetric measurement of the samples  
139 collected on polytetrafluoroethylene membrane filters (Chou et al. 2008). Sounding  
140 data (46734) were obtained from the CWB; the site on Penghu island was close to the





141 MG TEPA station (Fig. 1a).

142 During summer, the land-sea breeze easily combines with mountains' up/down  
143 slope wind during daytime/nighttime. As the sea breeze develops, air flows are typically  
144 transported from coastal areas and pass over the Taichung metropolitan region (Fig. 1c)  
145 coupled with mountain slope flow to the inland area. The Taichung metropolis is a large  
146 urban environment comprising residential, industrial, and agricultural lands (Cheng et  
147 al., 2009). In particular, Taichung Power Plant (TPP, Fig. 1c), which is coal-fired, and  
148 the Taichung Harbor Industrial (THI, Fig. 1c) zone are both located on the coast and  
149 are responsible for substantial emissions in central Taiwan. Thus, severe emission  
150 sources contribute to and affect the air quality in the Taichung metropolitan area under  
151 favorable weather conditions. For detailed information on the instruments used in the  
152 sampling analysis, please refer to Lee et al. (2019). Meteorological parameters,  
153 including wind speed and wind direction, temperature, and relative humidity were  
154 acquired from a meteorological station in the same location where data were collected  
155 for this study.

156

### 157 **3. Model configurations**

158 In this study, we used the Weather Research and Forecasting model (WRF)  
159 coupled with the WRF-Chem version 3.9 to study the air pollutants transport during  
160 the episode. We obtained the meteorological initial and boundary conditions for  
161 WRF-Chem from the National Center for Environmental Prediction (NCEP)  
162 Operational Global Forecast system  $0.25^\circ \times 0.25^\circ$  data sets at 6-h intervals. We  
163 selected the Yonsei University (YSU) planetary boundary layer (PBL) scheme for this



164 study. The coarse and fine domains had  $259 \times 370$  and  $301 \times 301$  grid nets with  
165 resolutions of 9 km and 3 km, respectively. The vertical had 41 levels, with the lowest  
166 level approximately 40 m above the surface. To ensure that the meteorological fields  
167 were well simulated, we employed the four-dimensional data assimilation scheme  
168 according to the NCEP-GFS data. Transport processes included advection by winds,  
169 convection by clouds, and diffusion by turbulent mixing. Removal processes included  
170 gravitational settling, surface deposition, and wet deposition (scavenging in  
171 convective updrafts and rainout or washout in large-scale precipitation). The kinetic  
172 preprocessor (KPP) interface was used in both the chemistry scheme of the Regional  
173 Atmospheric Chemistry Mechanism (Stockwell et al., 1990). The secondary organic  
174 aerosol formation module, the Modal Aerosol Dynamics Model for Europe (MADE)  
175 (Ackermann et al., 1998)/Volatility Basis Set (VBS) (Ahmadov et al., 2012) was  
176 employed in the WRF-Chem model.

177

## 178 **4. Results and discussion:**

### 179 **4.1 Characteristics of air quality over central Taiwan**

180 Figures 2a–c indicate the monthly mean concentration for  $PM_{10}$ ,  $PM_{2.5}$ , and  
181 daytime (08:00–17:00 LST) ozone between 1994 and 2019. Clear seasonal variations  
182 were noted for aerosol and ozone over central Taiwan. The lowest  $PM_{10}$ ,  $PM_{2.5}$ , and  
183 daytime ozone concentration were observed during summer (June–August) at 32–40  
184  $\mu\text{g}/\text{m}^3$ , 16–23  $\mu\text{g}/\text{m}^3$ , and 35–42 ppb, respectively. The concentration of daytime ozone



185 peaked in October, whereas  $PM_{10}$  and  $PM_{2.5}$  peaked in March. In general, the highest  
186 concentrations were observed in spring (March–May) and fall (September–November).  
187 The daytime ozone peaked at 56 ppb and 48 ppb in October and April, respectively (Fig.  
188 2c). For  $PM_{10}$  and  $PM_{2.5}$ , the peak concentrations were 70–75  $\mu\text{g}/\text{m}^3$  and 40–45  $\mu\text{g}/\text{m}^3$   
189 over the western plains in March (Fig. 2a, b). Regarding the characteristics of ozone  
190 distribution, the concentration at the mountain site was typically higher than that in  
191 urban areas and the coast. For  $PM_{10}$  and  $PM_{2.5}$ , the mountain site also typically had  
192 higher concentrations than did the urban and coastal areas, except during summer (Fig.  
193 2a,b). The monsoon dominates the prevailing wind over East Asia. During summer, a  
194 southwesterly wind prevails, whereas a northeasterly wind prevails during fall, winter,  
195 and spring. The characteristics of the seasonal variations might be due to the summer  
196 having a cleaner background and higher boundary layer height than those in other  
197 seasons. As mentioned earlier, the major emission sources such as industry and traffic  
198 are located in coastal and urban areas. The mean highest concentration of ozone  
199 typically occurs over rural mountain areas during summer; thus, the dominant land-sea  
200 breeze might play a critical role in the air quality in western Taiwan.

201 During summer (July only in this study) in 2017 and 2018, we conducted sampling  
202 campaigns in central Taiwan. Table 1 presents the mean concentration of the elements  
203 in  $PM_{2.5}$  at sampling stations SL, CSM, and ZS during July in 2017 and 2018. The mean  
204 concentration of  $PM_{2.5}$  for stations SL, CSM, and ZS were 15.7, 16.9, and 21.4  $\mu\text{g}/\text{m}^3$ .  
205 The inland rural mountain site, ZS, clearly had the highest total  $PM_{2.5}$  concentration.  
206 Organic carbon (OC) and  $\text{SO}_4^{2-}$  had the highest concentrations of the species in  $PM_{2.5}$ ,  
207 and both increased from the coast to the inland mountain area (Table 1). Because the  
208 major emissions were from coastal industry or urban areas, sea breeze transport played  
209 a role in  $PM_{2.5}$  concentration in the western plain. The major contributing species in



210  $PM_{2.5}$  were OC,  $SO_4^{2-}$ ,  $NO_3^-$ ,  $NH_4^+$ , and elemental carbon (EC; Table 1). At the coastal  
211 station SL, the concentrations of OC and  $SO_4^{2-}$  were comparable at  $4.3 \mu\text{g}/\text{m}^3$  and  $4.5$   
212  $\mu\text{g}/\text{m}^3$ , accounting for 27.5% and 28.6% of  $PM_{2.5}$ , respectively. At the city site CSM  
213 and the inland rural mountain station ZS, OC had concentrations of 5.6 (33.1% of  $PM_{2.5}$ )  
214 and  $6.6 \mu\text{g}/\text{m}^3$  (30.9% of  $PM_{2.5}$ ), respectively. The results indicated that the contribution  
215 of OC in  $PM_{2.5}$  could exceed 30% at the urban and inland mountain sites. The  
216 concentration of OC increased from the coast ( $4.3 \mu\text{g}/\text{m}^3$ ; 27.5% of  $PM_{2.5}$ ) to the  
217 mountain station ( $6.6 \mu\text{g}/\text{m}^3$ ; 30.9% of  $PM_{2.5}$ ), and the urban site had the highest  
218 proportion ( $5.6 \mu\text{g}/\text{m}^3$ ; 33.1% of  $PM_{2.5}$ ) in  $PM_{2.5}$  among these stations (Table 1).  $SO_4^{2-}$   
219 also exhibited an increased concentration from coastal areas to the inland mountain area,  
220 but the changes were minor ( $4.5\text{--}4.8 \mu\text{g}/\text{m}^3$ ). Notably, the proportion of  $SO_4^{2-}$  in  $PM_{2.5}$   
221 decreased from the coast to the mountain area because the major sources, TPP and THI  
222 (Fig. 1c), are located on the coast. The other species, namely  $NO_3^-$ ,  $NH_4^+$ , and EC, at  
223 SL, CSM, and ZS had comparable concentrations between stations (1.0–1.4, 1.7–2.0,  
224 and 1.1–1.4  $\mu\text{g}/\text{m}^3$ , respectively; Table 1). The inland rural station ZS was located in a  
225 foothill valley of the CMR and surrounded by mountains. Thus, the high concentration  
226 at ZS might be due to sea breeze transport.

227 In general, OC and  $SO_4^{2-}$  were the major species over western Taiwan, especially  
228 in inland areas. These results suggest that local contribution, such as traffic, industry,  
229 and even agricultural emissions, might play critical roles in the composition of  $PM_{2.5}$ .  
230 Furthermore, the spatial distributions of highest  $PM_{2.5}$  and daytime ozone concentration  
231 were not always in urban areas; instead, concentrations accumulated in inland rural  
232 areas (Fig. 2 and Table 1). The roles that the land-sea breeze, boundary layer  
233 development, and interaction of typhoon circulation with complex geographic  
234 structures play in air quality require clarification. The mechanism of these complex



235 processes and local circulation variations are demonstrated through a case study using  
236 numerical model simulation in Sect. 4.2.2.

## 237 **4.2 Air quality deterioration case from 15–17 July 2018**

### 238 **4.2.1 Weather condition and observation**

239 To explore air quality deterioration processes and formation mechanisms, we  
240 employed a severe air pollution episode between 15 and 17 July 2018. Weather maps  
241 obtained from the NCEP Global Forecast System (GFS) revealed that a tropical  
242 depression formed to the east of the Philippines and moved northwestward on 15 July  
243 2018 (Fig. 3a). Another low-pressure system followed, located to the south of this  
244 tropical depression on 16 July (Fig. 3b). On 17 July, this tropical depression  
245 strengthened and formed a weak typhoon named SONTINH, located between Taiwan  
246 and Luzon island in the Philippines (Fig. 3c); the original low-pressure system also  
247 strengthened into a tropical depression on 17 July. The continual formation of low-  
248 pressure systems or typhoons to the east of Luzon shifted the ambient wind flow of  
249 Taiwan to an easterly direction for an extended period between 15 and 17 July (Fig. 3a-  
250 c). The easterly ambient flow was easily blocked by Taiwan's CMR, resulting in a lee  
251 vortex formation associated with stable atmospheric conditions and weak wind speed  
252 in western Taiwan. The mechanism of lee vortex formation on the lee side of a high  
253 mountain has been described through a laboratory experiment (Hunt and Synder, 1980)  
254 and numerical modeling (e.g., Smolarkiewicz and Rotunno, 1989). Li and Chen (1998)



255 employed a wind flow with low Froude number ( $<0.5$ ) ( $Fr \equiv U/NH$ , where  $U$  is the far  
256 upstream flow speed;  $N$  is the Brunt–Vaisala frequency, a measure of stratification; and  
257  $H$  is the height of an obstacle), and the low-level airflow easily split off the northern  
258 coast and moved around the island of Taiwan. The current study is an example of a low  
259  $Fr$  case ( $<0.5$ ; assumed average wind speed,  $U = 10 \text{ ms}^{-1}$ ; Brunt–Vaisala frequency,  $N$   
260  $= 10^{-2} \text{ s}^{-1}$ ; and average mountain height,  $H = 2.5 \text{ km}$ ). Thus, we expected wind speeds to  
261 be weak and atmospheric conditions to be more stable on the lee side of the CMR  
262 compared with the windward side of eastern Taiwan.

263 Sounding data (Fig. 4) recorded at the CWB station in Penghu island (46734,  
264 close to MG in Fig. 1a) indicated a relatively weak wind speed ( $<5 \text{ m/s}$ ) in the low  
265 boundary (below 850 hPa) during the study period from 15 to 17 July 2018 (Fig.4a-c).  
266 Above 700 hPa (3000 m), a strong easterly wind ( $>10 \text{ m/s}$ ) prevailed due to the typhoon  
267 circulations. Furthermore, clear subsidence and multiple inversion layers were revealed  
268 in the sounding between 16 and 17 July (Fig. 4b,c). On 17 July, the inversion layer was  
269 even lower than 950 hPa (Fig. 4c); that is, only a few hundred meters over Penghu  
270 island in the Taiwan Strait. The sounding data revealed stable atmospheric conditions,  
271 high relative humidity, and weak wind speed on the leeside of the mountains over  
272 western Taiwan.

273 Figure 5 displays the variations in wind field and air pollutants (both  $\text{PM}_{2.5}$  and



274 ozone) at the TEPA stations on two small islands, KM and MG (locations marked in  
275 Fig. 1a) and results over the western plain from 12 to 18 July 2018. The wind direction  
276 and wind speed were quite different between these two stations and over the western  
277 plains (Fig. 5a). The wind speed was relatively strong at KM, especially between 16  
278 and 17 July because the typhoon circulation had already reached the coastal area of  
279 China and the Taiwan Strait. The wind direction was originally southerly on 12 July,  
280 becoming northeasterly after 12:00 LST on 14 July 2018. During periods of strong wind  
281 speed at KM, the concentrations of  $\text{PM}_{2.5}$  and  $\text{O}_3$  revealed no diurnal variation and a  
282 steady low, with  $\text{PM}_{2.5} < 15 \mu\text{g}/\text{m}^3$  and daytime  $\text{O}_3 < 40 \text{ ppb}$  after 12:00 LST on 14 July.  
283 The wind speed at MG was weaker than that at KM because MG is close to Taiwan and  
284 was likely affected by the mountain blocking effect mentioned earlier. Because the wind  
285 speed did not change considerably, the  $\text{PM}_{2.5}$  and  $\text{O}_3$  concentration levels did not  
286 fluctuate obviously at MG during the study period.

287 By contrast, the wind field time series indicated clear land–sea breeze variations  
288 over western Taiwan. At the inland mountain site, wind speed was relatively weak  
289 compared with the coastal and urban sites (Fig. 5a). The  $\text{PM}_{2.5}$  and ozone time series  
290 for the coastal, urban, mountain sites are presented in Fig. 5b-c. The  $\text{PM}_{2.5}$   
291 concentrations at the urban and mountain sites ranged from 30 to 60  $\mu\text{g}/\text{m}^3$  between 16  
292 and 17 July 2018. Notably, the timing of peak  $\text{PM}_{2.5}$  concentration differed between the



293 coastal, urban, and mountain sites. Peak  $PM_{2.5}$  at the coastal and urban sites was  
294 observed around noon, whereas peak  $PM_{2.5}$  at the inland mountain site occurred at 18:00  
295 LT on 17 July 2018 (Fig. 5b). The differences in the timing of the peak  $PM_{2.5}$   
296 concentrations between the coastal and urban sites and the inland mountain site could  
297 be attributed to the transport of the sea breeze. No clear diurnal variation in  $PM_{2.5}$   
298 concentration was observed between the urban and mountain sites between 16 and 17  
299 July. That is, even at night and in the early morning, the concentration remained as high  
300 as  $40 \mu\text{g}/\text{m}^3$  (Fig. 5b) because atmospheric conditions were favorable for air pollutant  
301 accumulation. The peak ozone concentration occurred around noon at the coast and  
302 urban sites, whereas the peak at the mountain site occurred later at 16:00 LST (Fig. 5c).  
303 We estimated that the concentrations of  $PM_{2.5}$  and ozone on the episode day on 17 July  
304 (Fig. 5b,c) were three times higher than the mean concentration during summer (Fig. 2)  
305 in central Taiwan. As mentioned earlier, the major emissions were generated by coastal  
306 industry and the Taichung city metropolitan area, but the peak ozone concentration  
307 occurred at the inland mountain station (120 ppb at PL) because of sea breeze transport  
308 from upstream to downstream sites.

309 Spatial distribution of wind field and  $PM_{2.5}$  concentration (Fig. 6) from TEPA  
310 stations in Taiwan revealed a strong easterly wind in northern and southern Taiwan and  
311 weak wind speed and clear sea breeze development during daytime in central Taiwan.





312  $PM_{2.5}$  concentrations remained low ( $<15 \mu\text{g}/\text{m}^3$ ) at the northern, eastern, and southern  
313 tips of Taiwan on 17 July 2018 (Fig. 6a-f). Over western Taiwan, a sea breeze developed  
314 after 10:00 LST, and a strong onshore flow blew air pollutants to the inland area (Fig. 6b-  
315 d). A high  $PM_{2.5}$  concentration ( $>50 \mu\text{g}/\text{m}^3$ ) extended from the coast to the urban area  
316 at noon (Fig. 6b-c), which was subsequently transported to the inland mountain area in  
317 the afternoon and nighttime (Fig. 6d-f). The high  $PM_{2.5}$  concentration accumulated in  
318 Maoli county (located north of Taichung city) at midnight owing to the convergence of  
319 southerly and land breeze (Fig. 6f). Actually, the spatial variation of  $PM_{2.5}$  could also  
320 be observed on the previous day (16 July; Fig. 5b), which contributed approximately  
321  $30 \mu\text{g}/\text{m}^3$  in the early morning on 17 July in central Taiwan.

322 The location of the high-pollution ozone was also strongly associated with the  
323 land-sea breeze during the daytime (Fig. 7 b-e). A high concentration of ozone was  
324 observed at the urban station at noontime (Fig. 7c); the ozone was transported to the  
325 inland mountain station, resulting in peak concentrations higher than 120 ppb between  
326 16:00 and 18:00 LST (Fig. 7d-f). By 22:00 LST, the ozone concentration had declined  
327 more rapidly in the city than in the mountain area because of the dilution effect (Fig. 7  
328 g-h). The detailed pollution process and mechanism are demonstrated and discussed in  
329 the model simulation in Sect. 4.2.2.

#### 330 **4.2.2 Simulation Results:**



331           The hourly comparison between observed (red solid) and simulated (blue dashed)  
332   PM<sub>2.5</sub> and ozone between 12 and 18 July 2018 are presented in Fig. 5b,c. In general,  
333   our simulation reasonably captured the variation of PM<sub>2.5</sub> and ozone in western Taiwan  
334   and small island sites, MG and KM (Table 2). For PM<sub>2.5</sub>, the root mean square error  
335   (RMSE) at all sites was less than 1.0 µg/m<sup>3</sup>, and the correlation between observed and  
336   simulated values was 0.72 and 0.81 at the urban and mountain sites, respectively.  
337   Regarding the mean bias of PM<sub>2.5</sub>, it was slightly overestimated at coastal and urban  
338   sites and underestimated at the mountain site and sites on the two islands. In the ozone  
339   simulation, the correlation between observed and simulated values was as high as 0.73–  
340   0.9, except for MG. The RMSE of ozone for all areas was less than 1.45 ppb. For the  
341   mean bias of ozone, the maximum underestimation (–10 ppb) occurred at the coastal  
342   site, and the maximum overestimation (13.8 ppb) occurred over the mountain area  
343   because of the simulation of the spatial distribution difference.

344           Figure 8 indicates the simulated wind field (streamline) and spatial distribution of  
345   PM<sub>2.5</sub> on 17 July 2018. The ambient wind flow was easterly and blocked by the CMR;  
346   the wind flow went around the CMR during the study period. The strongest wind speeds  
347   were recorded at the northern and southern tips of Taiwan and the coastal area of  
348   southeastern China (Fig. 8). By contrast, the wind speed was relatively weak on the lee  
349   side of the CMR from the middle of the Taiwan Strait to western Taiwan. This finding



350 is consistent with the observed wind speed being stronger at KM (Fig. 5a) than in the  
351 area over western Taiwan. Figure 8a–f reveals that the highest PM<sub>2.5</sub> concentration (>60  
352 μg/m<sup>3</sup>) occurred on the lee side of the CMR in central Taiwan during the daytime  
353 (08:00–16:00 LST) on 17 July 2018. After 08:00 LST, the sea breeze gradually  
354 developed and the onshore wind speed increased (Fig. 8a-c); thus, the high-  
355 concentration PM<sub>2.5</sub> plume was transported from the coast to the inland mountain area.  
356 Even though the area has high emissions, the PM<sub>2.5</sub> concentration along the coastal area  
357 of China was low because of the strong wind speed (Fig. 8a-c). As sea breeze developed  
358 after 08:00 LST, and the vortex circulation was coupled with the onshore flow (Fig. 8a–  
359 d). The lee vortex circulation was not clear because it combined with the sea breeze and  
360 enhanced the air pollutant transport to the inland area during the daytime. However, the  
361 lee vortex circulation was clearly formed in the area from 23.5 to 24.5 °N in the  
362 afternoon until early morning on the next day because the land breeze interacted with  
363 the mountain lee-side flows (Fig. 8e-f). After the lee vortex circulation formed, the  
364 southerly flow in the western plain was enhanced (Fig. 8e-f). These processes resulted  
365 in trapped air pollutants over the plain area because of the interaction between the lee  
366 vortex southerly component wind and the offshore flow in the nighttime and early  
367 morning. This also explains the absence of diurnal PM<sub>2.5</sub> variation and high  
368 concentration (>35 μg/m<sup>3</sup>) accumulated during nighttime and early morning on July 16



369 and 17 over central Taiwan (Figs. 5a,b, and 6f). Thus, the lee vortex formation was  
370 adverse to the development of the offshore flow (land breeze) and prolonged the air  
371 pollutant accumulation in western central Taiwan (Fig. 6 and 8). These critical  
372 processes explain why air pollutants tended to accumulate in central Taiwan during the  
373 episode days. Notably, the wind speed was strong and the concentration of  $PM_{2.5}$  was  
374 low in the Taiwan Strait close to coastal areas of China in the simulation (Fig. 8a-f) and  
375 according to observations at KM (Fig. 5a). According to the spatial distribution, a strong  
376 wind speed can limit the number of air pollutants transported southward from mainland  
377 China to Taiwan (Fig. 8b-f). That is, the pollution type was locally dominated during  
378 the event days.

379         Similar to the observed zone (Fig.7), the simulated ozone (Fig.9) was also  
380 dominated by circulations associated with the land-sea breeze and the interaction of the  
381 easterly flow with the CMR. Most of the area had steady low concentrations in the early  
382 morning on 17 July (Fig. 9a) because of the dilution effect of the ozone formation in  
383 the nighttime and early morning (Fig. 9a and h-i). A high concentration already existed  
384 over the mountain area in Miaoli County (Fig.1b) in the early morning at 04:00 LST  
385 (Fig. 9a), with a steady low concentration over the coastal and urban areas. During the  
386 daytime, the background ozone concentration was 25–35 ppb over the ocean. The ozone  
387 concentration promptly increased around noon and extended over almost the entire



388 western plains in the afternoon (Fig.9 c-f) on 17 July. The area of high ozone  
389 concentration extended over the western plains when the sea breeze developed after  
390 10:00 LST on 17 July (Fig. 9c). Following increases in wind speed, the high ozone  
391 concentration extended to the inland area and was transported further south of Taichung  
392 City (Fig. 9 d–e). The peak ozone concentration at the inland rural site occurred at 16:00  
393 LST, whereas it occurred in the city center at the urban site at 12-14:00 LST (Figs. 5c;  
394 7c,d; 9d,e). Because the major emission sources were coastal industry and the urban  
395 area, the high ozone concentration at the inland site was the result of ozone being  
396 transported by the sea breeze. The simulated peak ozone concentration occurred  
397 between 14:00 and 16:00 LST at the inland site because of the sea breeze coupled with  
398 the mountain upslope wind (Fig.9 c–f). Moreover, the high-ozone plume was associated  
399 with the lee vortex circulation over the Taiwan Strait and provided a southerly flow  
400 component during the nighttime and early morning (Fig. 9a, and g–i).

401 As mentioned earlier, sounding data indicated multiple inversion layers on the  
402 event days. To further investigate the boundary layer development and air pollutant  
403 distribution in the vertical, a northwest-southeast cross-section AA' (Fig.10a) was  
404 superimposed over the high concentration area, as illustrated in Fig. 10. In the early  
405 morning at 05 LST (Fig.10b), a separate high-concentration plume was observed at  
406 ground level and another remained at an elevation of 1000 m on 17 July. It is a typical



407 boundary layer structure due to ground surface radiation cooling under stable  
408 atmospheric conditions during nighttime and early morning. These two layers' plume  
409 coupled together due to boundary layer gradually developed in the morning after 0700  
410 LST(Fig.10 b-d). Because the emissions increased during rush hour, the concentration  
411 promptly increased as the PM<sub>2.5</sub> plumes of these two layers coupled well in the vertical  
412 below 1000 m at 10:00 LST (Fig. 10 d). The wind speed was weak at elevations below  
413 1500 m but strong and offshore in a southeast-northwest direction above 2000 m due to  
414 easterly tropical cyclone circulation. The high-PM<sub>2.5</sub> plume (concentration > 50 µg/m<sup>3</sup>)  
415 was pushed by the sea breeze coupled with the upslope wind and accumulated in the  
416 inland rural area during daytime (12:00–16:00 LST) (Fig. 10e–g). The highest  
417 concentration was not at ground level but heights between 500 and 1000 m at noontime  
418 (Fig.10e) and 1000-1500 m in the afternoon (Fig. 10 f-g). The boundary layer structure  
419 and the coupled between sea breeze and mountain upslope wind played important roles  
420 for the PM<sub>2.5</sub> concentration distribution in the vertical along the cross-section (Fig.10d-  
421 g). As offshore wind developed, which pushed the air pollutants from the mountain area  
422 to the plain and coastal area (Fig. 10 g–i), and the elevation of the plume was  
423 predominantly between 500 and 1500 m after 20:00 LST. The discussion above  
424 indicated that PM<sub>2.5</sub> concentration was not only strongly related to the interaction of  
425 ambient flow with the CMR but also the diurnal variations in boundary layer



426 development.

427 Figure 11 indicates the ozone cross-section in a northwest-southeast direction in  
428 Fig. 10a. A low ozone concentration (<25 ppb) was observed near ground level because  
429 of the dilution effect in the early morning at 04:00 LST (Fig. 11a) on 17 July. However,  
430 a high-ozone layer was observed between 500 and 1500 m because of the previous  
431 day's contribution. After 08:00 LST, the mixing layer developed, and emissions from  
432 traffic and industry also increased. Concurrently, both the onshore sea breeze over the  
433 plain and the upslope wind over the mountain developed; thus, wind speed also  
434 enhanced in the low boundary (Fig. 11b-e). The sea breeze and weak wind speed also  
435 exacerbated the high-concentration ozone in the inland area during the daytime (Fig.  
436 11c-f). At nighttime, the ozone concentration gradually decreased because of the  
437 dilution effect below 500 m (Fig. 11h-i). However, TEPA measurements revealed that  
438 a layer with high ozone concentration remained between 1000 and 1500 m (Fig. 7g-h)  
439 because low  $\text{NO}_x$  was emitted over the mountain area in Taichung and Miaoli county.  
440 This also explains why the high ozone concentration first occurred over the mountain  
441 slope area as a result of the concurrent sea breeze and upslope wind in the morning  
442 (Figs. 9a and 11a). That is, the area of high concentration occurred earlier in the low-  
443 emission mountain area than on the plains, a major emission area. The simulated ozone  
444 concentration indicated that the high concentration did not occur near ground level but



445 at 800–1000 m. This phenomenon was closely related to the development of the  
446 boundary layer structure and its interaction with the upper residual layer formation on  
447 the previous day.

#### 448 **5. Discussion:**

449 The wind direction over Taiwan during summer is mostly southerly to  
450 southwesterly (Table 1). However, the wind direction during the episode was westerly  
451 to northwesterly (Table 2). The wind direction changed because of the critical  
452 interaction between typhoon circulations and the CMR. Moreover, the concentration of  
453  $PM_{2.5}$  and its composition during the episode also differed significantly from the  
454 monthly mean, as revealed in Table 2. A substantial increase in daily mean  $PM_{2.5}$  was  
455 observed at all sites, especially at the CSM site (urban), where concentration increased  
456 from 16.9 to 40.5  $\mu\text{g}/\text{m}^3$  (Table 2). Furthermore,  $\text{SO}_4^{2-}$  became the dominant species in  
457  $PM_{2.5}$  from the coastal to the mountain area, ranging from 30.5 to 29.7% during the  
458 episode. The  $\text{SO}_4^{2-}$  concentration during the episode (Table 2) was more than twice that  
459 of the monthly mean (Table 1) in the Taichung area. This variation was due to the wind  
460 direction changing from southwesterly to northwesterly, resulting in a contribution  
461 increase from the upstream TPP and THI (Fig. 1c), which are the major sources in  
462 central Taiwan.

463 On 17 July 2018, Taichung City not only experienced high air pollutant





464 concentrations but also a maximum air temperature as high as 35.4 °C. That is, a heat  
465 wave (Lin et al., 2017; Kuth et al. 2017) occurred on 17 July because of the subsidence  
466 of the typhoon circulation on the lee side of the mountain. The daily mean temperature  
467 for the sampling sites between 15 and 17 July for SL, CSM, and ZS were 29.9 °C, 30  
468 °C, and 29.4 °C, respectively. However, the monthly mean temperatures (July in 2017  
469 and 2018) during the sampling period for SL, CSM, and ZS were 28.9°C, 28.8°C, and  
470 26.5°C, respectively. Thus, the daily mean temperature during the episode period was  
471 1–2 °C higher than is typical for days in July. In general, the mean wind speed on the  
472 episode days at these three sites was weaker (<1 m/s) than the monthly mean (Tables 1  
473 and 2). Such stable weather conditions, weak wind speed, and high air temperature were  
474 conducive to the generation and formation of a secondary aerosol. This is exemplified  
475 by the concentrations of other species, such as OC, NO<sub>3</sub><sup>-</sup> and NH<sub>4</sub><sup>+</sup>, being considerably  
476 higher during the episode days (Table 2) compared with the monthly mean in Table 1.  
477 Notably, EC increased to a lesser extent than did the other species. These results suggest  
478 that secondary aerosol plays a critical role under such stable weather conditions and  
479 wind direction. Because ambient wind changes during typhoon formation between  
480 Taiwan and Luzon island in the Philippines are not uncommon, the air quality impacts  
481 in such weather conditions merit further research. A detailed discussion of variations in  
482 aerosol chemical composition transformation will be presented in a separate paper.



483 **6. Summary:**

484       The lowest air pollution levels in Taiwan typically occur during summer because  
485 of a low air pollution background under southwesterly prevailing winds and the higher  
486 boundary elevation associated with high air temperatures. The monthly mean  
487 concentrations of PM<sub>10</sub>, PM<sub>2.5</sub>, and daytime ozone (08:00–17:00 LT) in summer (June–  
488 August) during 2004-2019 over central Taiwan are 35–40 µg/m<sup>3</sup>, 18–22 µg/m<sup>3</sup>, and 30–  
489 42 ppb, respectively. Sampling analysis also indicated that the contribution of OC in  
490 PM<sub>2.5</sub> could exceed 30% in urban and inland mountain sites. However, episodes of  
491 poor air quality frequently occur over the western plains when an easterly typhoon  
492 circulation interacts with the complex topographic structure in Taiwan. Under such a  
493 weather condition, concentrations of PM<sub>2.5</sub> and ozone could be higher than 2 times of  
494 those monthly mean. During the episode, SO<sub>4</sub><sup>2-</sup> became the major contributor to PM<sub>2.5</sub>,  
495 and its concentration and contribution proportion (%) in PM<sub>2.5</sub> at coastal, urban, and  
496 mountain sites were 9.4 µg/m<sup>3</sup> (30.5%), 12.1 µg/m<sup>3</sup> (29.9%), and 11.6 µg/m<sup>3</sup> (29.7%),  
497 respectively. It is due to the northwesterly wind was conducive to the transport of SO<sub>2</sub>  
498 and sulfate from the coastal upstream major emission sources (areas in TPP and THI)  
499 to the inland area.

500       To explore the mechanism of air pollution formation, we conducted a detailed  
501 data analysis and WRF-chem model simulation of an episode of poor air quality



502 between 15 and 17 July 2018. Numerical modeling indicated that not only wind  
503 direction changes due to lee vortex but also boundary layer development were the key  
504 mechanisms in the transport of air pollutants. Typhoons are a frequent occurrence in the  
505 area around Taiwan during summer and fall. Because of Taiwan's complex  
506 geographic structure, the flow patterns and diurnal boundary layer variations resulted  
507 in the high concentrations of ozone and PM<sub>2.5</sub> and composition of PM<sub>2.5</sub> during the  
508 episode deviating from the monthly mean in summer. The results of this study  
509 contribute valuable data on the effect of extreme weather, such as typhoon circulation,  
510 on the weather parameters and air quality in Taiwan. We summarize the key  
511 mechanisms and processes of the interaction between, typhoon circulation, lee vortex,  
512 land-sea breeze, boundary layer development, and topography and their effects on air  
513 quality in Fig. 12.

514 (1)First, typhoon circulations provided a strong easterly ambient flow. This easterly  
515 flow interacted with the CMR, resulting in a lee vortex formation over western  
516 Taiwan. (Fig.12, left panel)

517 (2)During the nighttime, the offshore wind that developed pushed the air pollutants  
518 from the mountain area to the plain and coastal areas. Concurrently, a clear lee  
519 vortex formation could be observed near Taiwan's coastal area in the Taiwan  
520 Strait and thus a southerly flow in the western plains was enhanced. These



521 processes resulted in trapped air pollutants over the Taichung area and the  
522 mountain area in Miaoli county (Fig. 1b) in western Taiwan. The boundary layer  
523 height was low because of ground surface radiation cooling and inversion layer  
524 formation. The air pollutants remained separate because of considerable  
525 decreases in emissions at ground level coupled with the boundary residual layer  
526 being at a higher elevation. (Fig.12, right top panel)

527 (3)In the morning, this residual layer with polluted air mass combined with and  
528 contributed to the ground surface air concentration level because the boundary  
529 layer height increased. This also explains why the ozone and  $PM_{2.5}$  concentrations  
530 dramatically increased after the boundary layer development during the daytime.  
531 For this reason, the high-concentration ozone plume was located in a low-  
532 emission mountain area and the episode occurred at an earlier time than in the  
533 plain area where the major emission sources are located.

534 During the daytime, the lee vortex flow coupled with a sea breeze and combined  
535 with a mountain upslope wind; this resulted in the accumulation of air pollutants  
536 in the inland mountain area. Furthermore, because of the mountain upslope flow,  
537 the high  $PM_{2.5}$  and ozone concentrations were located not at ground level but at  
538 heights between 500 and 1000 m. The peak concentration at the inland mountain  
539 site occurred approximately 4–6 hours later than at the upstream coastal site



540 because of the sea breeze. (Fig.12 right down panel)

541 **Acknowledgements:**

542 The accomplishment of this work has financial support from the Ministry of Science  
543 and Technology, Taiwan, under grants 108-2111-M-001-002 and 109-2111-M-001-004.

544

545 **References:**

546 Ackermann, I. J., Hass, H., Memmsheimer, M., Ebel, A., Binkowski, F. S., and Shankar,  
547 U.: Modal aerosol dynamics model for Europe: development and first applications,  
548 *Atmos. Environ.*, 32, 2981–2999, [https://doi.org/10.1016/S1352-2310\(98\)00006-5](https://doi.org/10.1016/S1352-2310(98)00006-5),  
549 1998.

550 Ahmadov, R., McKeen, S. A., Robinson, A. L., Bahreini, R., Middlebrook, A. M., de  
551 Gouw, J. A., Meagher, J., Hsie, E.-Y., Edgerton, E., Shaw, S., and Trainer, M.: A  
552 volatility basis set model for summertime secondary organic aerosols over the  
553 eastern United States in 2006, *J. Geophys. Res.*, 117,  
554 <https://doi.org/10.1029/2011JD016831>, 2012.

555 Chang, L. T.-C., Tsai, J.-H., Lin, J.-M., Huang, Y.-S., and Chiang, H.-L.: Particulate  
556 matter and gaseous pollutants during a tropical storm and air pollution episode in  
557 Southern Taiwan, *Atmos. Res.*, 99, 67–79,  
558 <https://doi.org/10.1016/j.atmosres.2010.09.002>, 2011.

559 Cheng, M. T., Horng, C. L., Su, Y. R., Lin, L. K., Lin, Y. C., and Chou, C. C.-K.:  
560 Particulate matter characteristics during agricultural waste burning in Taichung City,  
561 Taiwan, *J. Hazard. Mater.*, 165, 187–192,  
562 <https://doi.org/10.1016/j.jhazmat.2008.09.101>, 2009.

563 Cheng, W. L., Lai, L. W., Den, W., Wu, M. T., Hsueh, C. A., Lin, P. L., Pai, C. L., and



- 564 Yan, Y. L.: The relationship between typhoons' peripheral circulation and ground-  
565 level ozone concentrations in central Taiwan, *Environ. Monit. Assess.*, 186, 791–  
566 804, <https://doi.org/10.1007/s10661-013-3417-7>, 2014.
- 567 Chou, C. C.-K., Lee, C. T., Yuan, C. S., Hsu, W.C., Lin, C. Y., Hsu, S. C., and Liu, S.  
568 C.: Implications of the chemical transformation of Asian outflow aerosols for the  
569 long-range transport of inorganic nitrogen species. *Atmos. Environ.*, 42, 7508–7519,  
570 <https://doi.org/10.1016/j.atmosenv.2008.05.049>, 2008.
- 571 Chow, E. C. H., Li, R. C. Y., and Zhou, W.: Influence of tropical cyclones on Hong  
572 Kong air quality, *Adv. Atmos. Sci.*, 35, 1177–1188, [https://doi.org/10.1007/s00376-](https://doi.org/10.1007/s00376-018-7225-4)  
573 018-7225-4, 2018.
- 574 Deng, T., Wang, T., Wang, S., Zou, Y., Yin, C., Li, F., Liu, L., Wang, N., Song, L., Wu,  
575 C., and Wu, D.: Impact of typhoon periphery on high ozone and high aerosol  
576 pollution in the Pearl River Delta region, *The Scie. Total Environ.*, 668, 617-630,  
577 <https://doi.org/10.1016/j.scitotenv.2019.02.450>, 2019.
- 578 Ding, A. J., Wang, T., Zhao, M., Wang, T. J., and Li, Z. K.: Simulation of sea-land  
579 breezes and a discussion of their implications on the transport of air pollution during  
580 a multiday ozone episode in the Pearl River Delta of China, *Atmos. Environ.*, 38,  
581 6737–6750, <https://doi.org/10.1016/j.atmosenv.2004.09.017>, 2004.
- 582 Fang, G. C., Lin, S. J., Chang, S. Y., Chou, C. C.-K.: Effect of typhoon on atmospheric  
583 particulates in autumn in central Taiwan, *Atmos. Environ.*, 43, 6039–6048,  
584 <https://doi.org/10.1016/j.atmosenv.2009.08.033>, 2009.
- 585 Feng, Y., Wang, A., Wu, D., and Xu, X.: The influence of tropical cyclone Melor on  
586 PM10 concentrations during an aerosol episode over the Pearl River Delta region of  
587 China: numerical modeling versus observational analysis, *Atmos. Environ.*, 41,  
588 4349–4365, <https://doi.org/10.1016/j.atmosenv.2007.01.055>, 2007.
- 589 Grell, G. A., Peckham, S. E., Schmitz, R., McKeen, S. A., Frost, G., Skamarock, W. C.,



- 590 and Eder, B.: Fully coupled “online” chemistry within the WRF model, *Atmos.*  
591 *Environ.*, 39, 6957–6975, <https://doi.org/10.1016/j.atmosenv.2005.04.027>, 2005.
- 592 Hsu, C. H., and Cheng, F. Y.: Synoptic Weather Patterns and Associated Air Pollution  
593 in Taiwan, *Aerosol Air Qual. Res.*, 19, 1139–1151,  
594 <https://doi.org/10.4209/aaqr.2018.09.0348>, 2019.
- 595 Huang, J. P., Fung, J. C. H., Lau, A. K. H., and Qin, Y.: Numerical simulation and  
596 process analysis of typhoon-related ozone episodes in Hong Kong, *J. Geophys. Res.*,  
597 101, <https://doi.org/10.1029/2004JD004914>, 2005.
- 598 Huang, J. P., Fung, J. C. H., and Lau, A. K. H.: Integrated processes analysis and  
599 systematic meteorological classification of ozone episodes in Hong Kong, *J.*  
600 *Geophys. Res.*, 111, <https://doi.org/10.1029/2005JD007012>, 2006.
- 601 Huang, T., Yang, Y., O’Connor, E. J., Lolli, S., Haywood, J., Osborne, M., Cheng, J.  
602 C.-H., Guo, J., Yim, S. H.-L.: Influence of a weak typhoon on the vertical  
603 distribution of air pollution in Hong Kong: A perspective from a Doppler LiDAR  
604 network, *Environ. Pollut.*, 276, 116534,  
605 <https://doi.org/10.1016/j.envpol.2021.116534>, 2021.
- 606 Hunt, C. R. and Snyder, W. H.: Experiments on stably and neutrally stratified flow over  
607 a model three-dimensional hill, *J. Fluid Mech.*, 96, 671–704,  
608 <https://doi:10.1017/S0022112080002303>, 1980.
- 609 Jiang, Y. C., Zhao, T. L., Liu, J., Xu, X. D., Tan, C. H., Cheng, X. H., Bi, X. Y., Gan,  
610 J. B., You, J. F., and Zhao, S. Z.: Why does surface ozone peak before a typhoon  
611 landing in southeast China?, *Atmos. Chem. Phys.*, 15, 13331–13338,  
612 <https://doi.org/10.5194/acp-15-13331-2015>, 2015.
- 613 Kueh, M. T., Lin, C. Y., Chuang, Y. J., Sheng, Y. F., and Chien, Y. Y.: Climate  
614 variability of heat waves and their associated diurnal temperature range variations  
615 in Taiwan, *Environ. Res. Lett.*, 12, 074017, <https://doi.org/10.1088/1748->



- 616 9326/aa70d9, 2017.
- 617 Lam, Y. F., Cheung, H. M., and Ying, C. C.: Impact of tropical cyclone track change  
618 on regional air quality, *Sci. Total Environ.*, 610–611, 1347–1355,  
619 <https://doi.org/10.1016/j.scitotenv.2017.08.100>, 2018.
- 620 Lee, C. S. L., Chou, C. C.-K., Cheung, H. C., Tsai, C.-Y., Huang, W.-R., Huang, S.-H.,  
621 Chen, M.-J., Liao, H.-T., Wu, C.-F., Tsao, T.-M., Tsai, M.-J., and Su, T.-C.:  
622 Seasonal variation of chemical characteristics of fine particulate matter at a high-  
623 elevation subtropical forest in East Asia, *Environ. Pollut.*, 246, 668–677,  
624 <https://doi.org/10.1016/j.envpol.2018.11.033>, 2019.
- 625 Lee, Y. C., Calori, G., Hills, P., and Carmichael, G. R.: Ozone episodes in urban Hong  
626 Kong 1994–1999, *Atmos. Environ.*, 36, 1957–1968, [https://doi.org/10.1016/S1352-2310\(02\)00150-4](https://doi.org/10.1016/S1352-2310(02)00150-4), 2002.
- 628 Li, J. and Chen, Y.-L.: Barrier jets during TAMEX, *Mon. Weather Rev.*, 126, 959–971,  
629 [https://doi.org/10.1175/1520-0493\(1998\)126<0959:BJDT>2.0.CO;2](https://doi.org/10.1175/1520-0493(1998)126<0959:BJDT>2.0.CO;2), 1998.
- 630 Lin, C. Y. and Chen, C. S.: A study of orographic effects on mountain-generated  
631 precipitation systems under weak synoptic forcing, *Meteorol. Atmos. Phys.*, 81, 1–  
632 25, <https://doi.org/10.1007/s007030200028>, 2002.
- 633 Lin, C. Y., Wang, Z., Chou, C. C.-K., Chang, C.-C., and Liu, S. C.: A numerical study  
634 of an autumn high ozone episode over southwestern Taiwan, *Atmos. Environ.*, 41,  
635 3684–3701, <https://doi.org/10.1016/j.atmosenv.2006.12.050>, 2007b.
- 636 Lin, C. Y., Hsu, H. M., Sheng, Y. F., Kuo, C. H., and Liou, Y. A.: Mesoscale processes  
637 for super heavy rainfall of Typhoon Morakot (2009) over southern Taiwan, *Atmos.*  
638 *Chem. Phys.*, 11, 345–361, <https://doi.org/10.5194/acp-11-345-2011>, 2011.
- 639 Lin, C. Y., Chien, Y. Y., Su, C. J., Kueh, M. T., and Lung, S. C.: Climate variability of  
640 heat wave and projection of warming scenario in Taiwan, *Clim. Chang.*, 145, 305–  
641 320, <https://doi.org/10.1007/s10584-017-2091-0>, 2017.





- 642 Luo, M., Hou, X., Gu, Y., Lau, N.-C., and Yim, S. H.-L.: Trans-boundary air pollution  
643 in a city under various atmospheric conditions, *Sci. Total Environ.*, 618, 132–141,  
644 <https://doi.org/10.1016/j.scitotenv.2017.11.001>, 2018.
- 645 Shu, L., Xie, M., Wang, T., Gao, D., Chen, P., Han, Y., Li, S., Zhuang, B., and Li, M.:  
646 Integrated studies of a regional ozone pollution synthetically affected by subtropical  
647 high and typhoon system in the Yangtze River Delta region, China, *Atmos. Chem.*  
648 *Phys.*, 16, 15801–15819, <https://doi.org/10.5194/acp-16-15801-2016>, 2016.
- 649 Smolarkiewicz, K. S. and Rotunno, R.: Low Froude number flow past three-  
650 dimensional obstacles. Part I: baroclinically generated lee vortices, *J. Atmos. Sci.*,  
651 46, 1154–1164, [https://doi.org/10.1175/1520-0469\(1989\)046<1154:LFNFPT>2.0.CO;2](https://doi.org/10.1175/1520-0469(1989)046<1154:LFNFPT>2.0.CO;2), 1989.
- 653 Stockwell, W. R., Middleton, P., Chang, J. S., and Tang, X.: The second generation  
654 regional acid deposition model chemical mechanism for regional air quality  
655 modeling, *J. Geophys. Res.*, 95, 16343–16367,  
656 <https://doi.org/10.1029/JD095iD10p16343>, 1990.
- 657 Tu, J. Y., and Chen, J. M.: Large-scale indices for assessing typhoon activity around  
658 Taiwan, *Int. J. Climatol.*, 39, 921–33, <https://doi.org/10.1002/joc.5852>, 2019.
- 659 Wei, X., Lam, K.-S., Cao, C., Li, H., and He, J.: Dynamics of the Typhoon Haitang  
660 related high ozone episode over Hong Kong, *Adv. Meteorol.*, 2016, 6089154,  
661 <https://doi.org/10.1155/2016/6089154>, 2016.
- 662 Yan, J., Chen, L., Lin, Q., Zhao, S., and Zhang, M.: Effect of typhoon on atmospheric  
663 aerosol particle pollutants accumulation over Xiamen, China, *Chemosphere*, 159,  
664 244–255, <https://doi.org/10.1016/j.chemosphere.2016.06.006>, 2016.
- 665 Yang, J. X., Lau, A. K. H., Fung, J. C. H., Zhou, W., and Wenig, M.: An air pollution  
666 episode and its formation mechanism during the tropical cyclone Nuri’s landfall in  
667 a coastal city of south China, *Atmos. Environ.*, 54, 746–753,



668 <https://doi.org/10.1016/j.atmosenv.2011.12.023>, 2012.

669 Zhang, X., Liu, Y., Deng, X., Chen, P., Feng, Y., Fan, Q.: Analysis of Summertime  
670 Typical Pollution in Pearl River Delta Region-Numerical Simulation of  
671 Meteorological Field, *Meteorol. Environ. Res.*, 59, 9–18,  
672 [https://search.proquest.com/scholarly-journals/analysis-summertime-typical-](https://search.proquest.com/scholarly-journals/analysis-summertime-typical-pollution-pearl-river/docview/1531993540/se-2?accountid=13877)  
673 [pollution-pearl-river/docview/1531993540/se-2?accountid=13877](https://search.proquest.com/scholarly-journals/analysis-summertime-typical-pollution-pearl-river/docview/1531993540/se-2?accountid=13877), 2014.

674 Zhang, Y., Mao, H. T., Ding, A. J., Zhou, D. R., and Fu, C. B.: Impact of synoptic  
675 weather patterns on spatio-temporal variation in surface O<sub>3</sub> levels in Hong Kong  
676 during 1999–2011, *Atmos. Environ.*, 73, 41–50,  
677 <https://doi.org/10.1016/j.atmosenv.2013.02.047>, 2013.

678

679

680

681

682

683

684

685

686

687

688

689

690

691

692

693



694

695 Table 1: Concentrations of PM<sub>2.5</sub> and its major components and daytime ozone as  
 696 well as meteorological parameters at the SL (coastal), CSM (urban), and ZS  
 697 (mountain) sampling sites in July 2017 and 2018.

	201707 201807					
	Coast (SL)		Urban (CSM)		Mountain (ZS)	
	Value	(%)	Value	(%)	Value	(%)
PM <sub>2.5</sub> (µg/m <sup>3</sup> )	15.7		16.9		21.4	
SO <sub>4</sub> <sup>2-</sup> (µg/m <sup>3</sup> )	4.5	(28.6%)	4.6	(27.5%)	4.8	(22.2%)
OC (µg/m <sup>3</sup> )	4.3	(27.5%)	5.6	(33.1%)	6.6	(30.9%)
NO <sub>3</sub> <sup>-</sup> (µg/m <sup>3</sup> )	1.4	(9.1%)	1.0	(6.0%)	1.1	(5.3%)
NH <sub>4</sub> <sup>+</sup> (µg/m <sup>3</sup> )	1.7	(10.5%)	1.7	(9.9%)	2.0	(9.3%)
EC (µg/m <sup>3</sup> )	1.1	(6.7%)	1.1	(6.3%)	1.4	(6.4%)
O <sub>3</sub> (ppb, 08-17LST)	35.3		39.4		39.7	
T (°C)	28.9		28.8		26.5	
ws (m/s)	0.7		0.9		0.5	
wd (°)	207.7		238.4		247.5	

698

699

700 Table 2: Concentrations of PM<sub>2.5</sub> and its major components and daytime ozone as  
 701 well as meteorological parameters at the SL (coastal), CSM (urban), and ZS  
 702 (mountain) sampling sites between 15 and 17 July 2018.

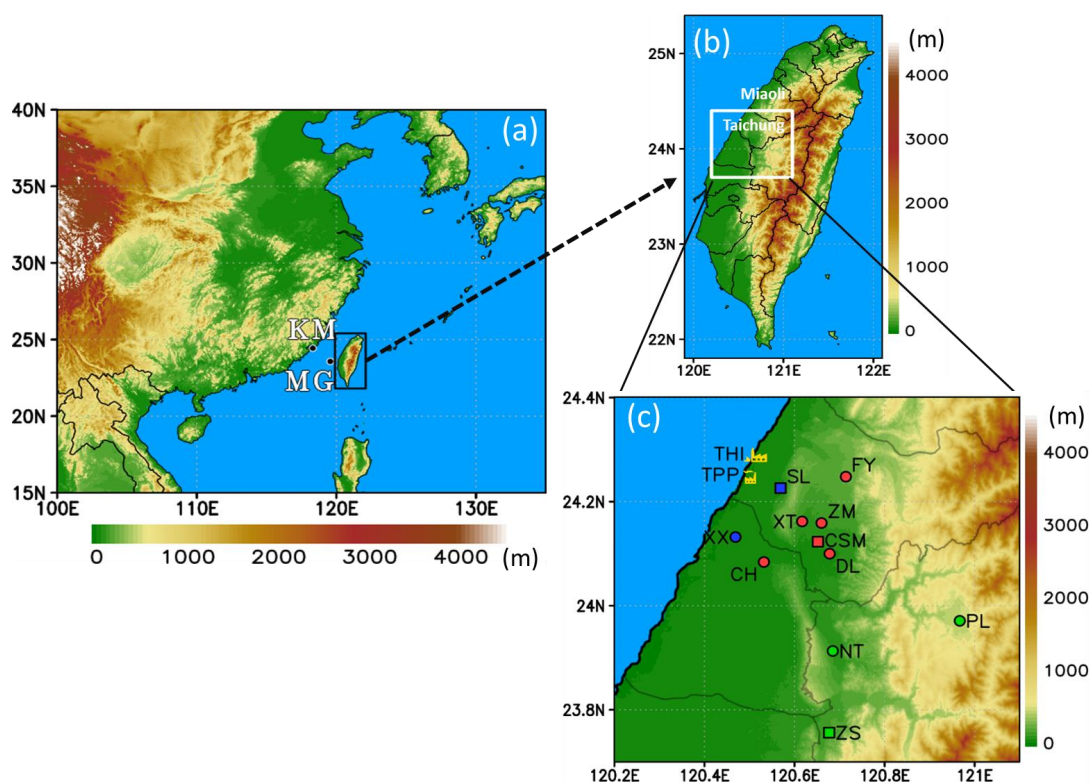
	2018/07/15-2018/07/17					
	Coast (SL)		Urban (CSM)		Mountain (ZS)	
	Value	(%)	Value	(%)	Value	(%)
PM <sub>2.5</sub> (µg/m <sup>3</sup> )	30.9		40.5		39.2	
SO <sub>4</sub> <sup>2-</sup> (µg/m <sup>3</sup> )	9.4	(30.5%)	12.1	(29.9%)	11.6	(29.7%)
OC (µg/m <sup>3</sup> )	6.9	(22.2%)	9.7	(23.8%)	8.1	(20.7%)
NO <sub>3</sub> <sup>-</sup> (µg/m <sup>3</sup> )	2.9	(9.5%)	2.9	(7.0%)	4.4	(11.1%)
NH <sub>4</sub> <sup>+</sup> (µg/m <sup>3</sup> )	4.0	(12.9%)	4.7	(11.7%)	5.9	(15.0%)
EC (µg/m <sup>3</sup> )	1.8	(6.0%)	1.5	(3.6%)	2.0	(5.2%)
O <sub>3</sub> (ppb, 08-17LST)	65.5		74.1		64.7	
T (°C)	29.9		30.0		29.4	
ws (m/s)	0.6		0.9		0.8	
wd (°)	290.6		250.7		279.9	

703

704



705  
706  
707  
708  
709  
710  
711



712  
713  
714  
715  
716  
717  
718  
719  
720  
721  
722

Fig. 1. (a) Location of Taiwan and surrounding countries in East Asia. KM and MG are the island stations of the Taiwan Environmental Protection Administration (TEPA). (b) Topography over Taiwan and the locations of Taichung city and Miaoli county. (c) Location of TEPA air quality monitoring stations in central Taiwan in coastal (SL and XX), urban (FY, XT, ZM, CH, and DL), and mountain (PL, NT, and ZS) areas. TPP, Taichung Power Plant; THI, Taichung Harbor Industrial area.



723

724 (a)

725

726

727

728

729

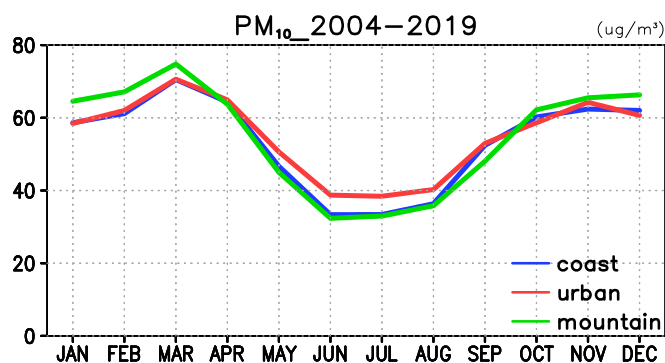
730

731

732

733

734



735 (b)

736

737

738

739

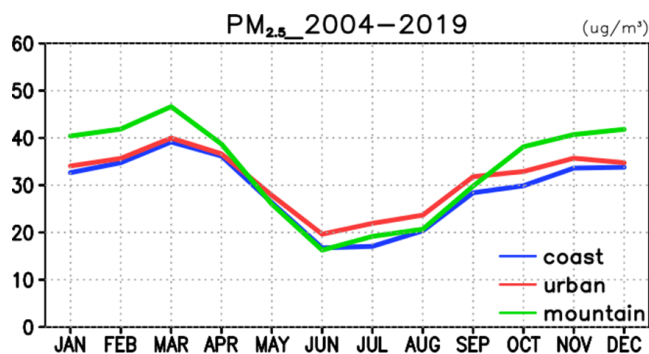
740

741

742

743

744



745 (c)

746

747

748

749

750

751

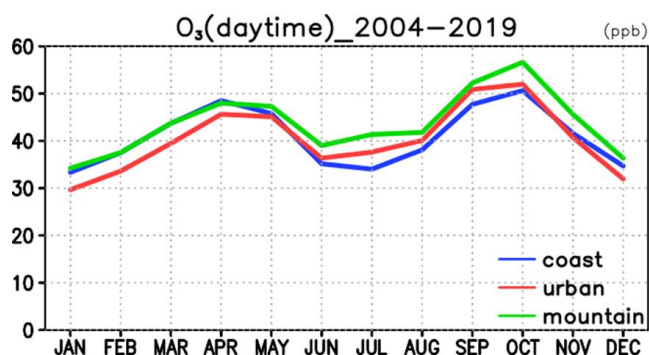
752

753

754

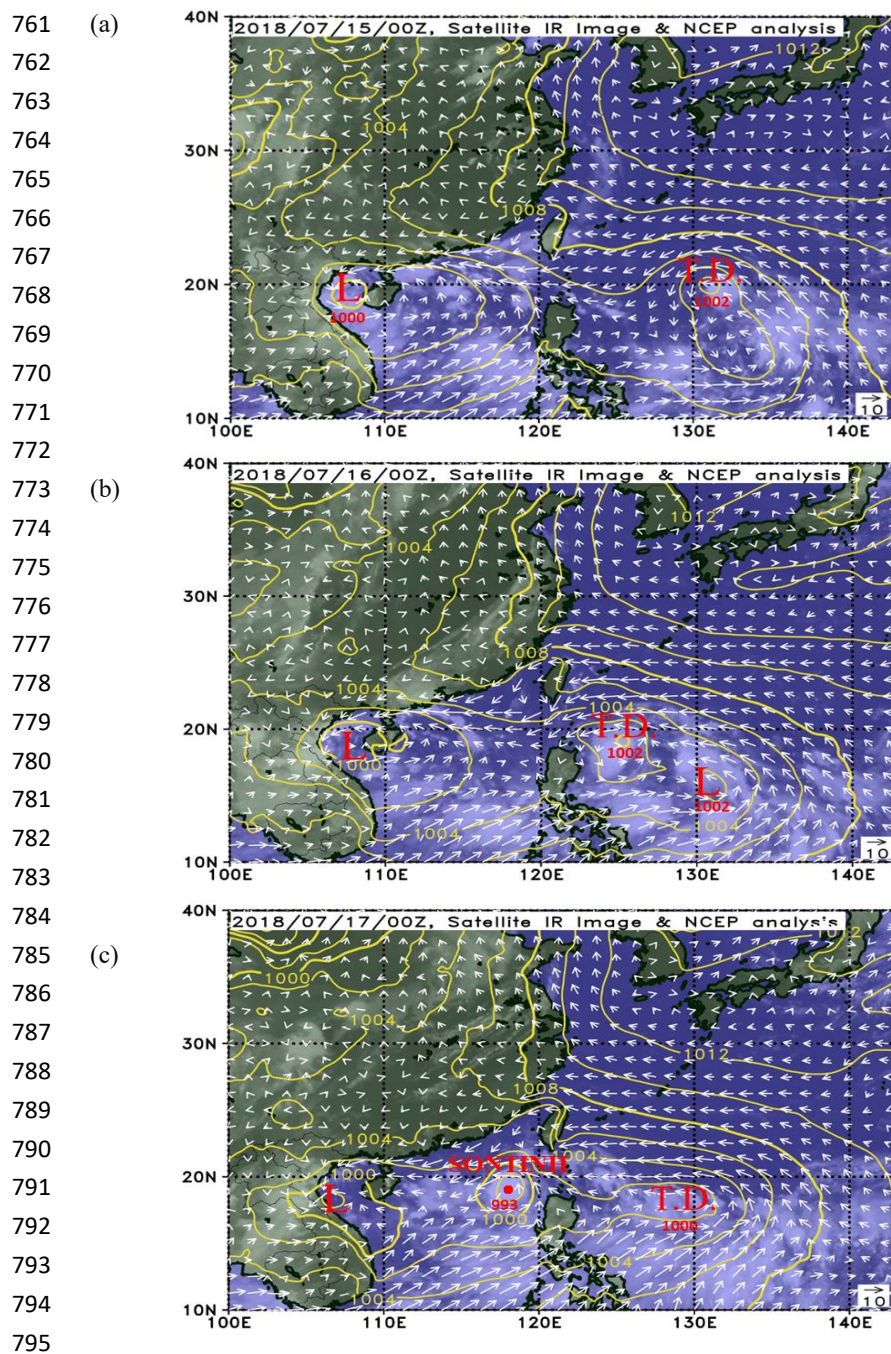
755

756



757 Fig. 2. Average monthly concentrations of (a) PM<sub>10</sub>, (b) PM<sub>2.5</sub>, and (c) daytime  
758 (08:00–17:00 LST) ozone for coastal, urban, and mountain areas between 2004 and  
759 2019.

760

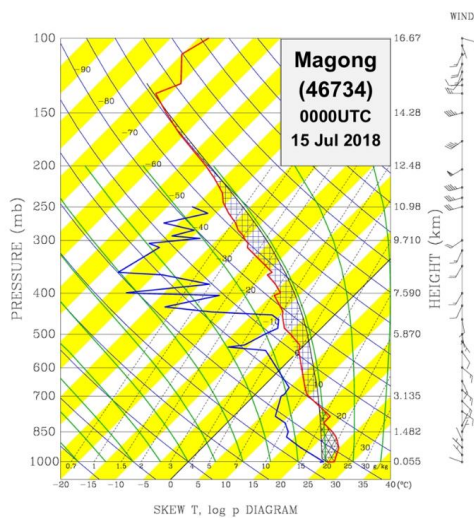


796 Fig. 3. Near-surface weather charts obtained from NCEP GFS data. Gray area  
797 represents cloud area according to a Himawari satellite infrared image. (a) 00:00  
798 UTC, 15 July; (b) 00:00 UTC, 16 July; and (c) 00:00 UTC, 17 July.

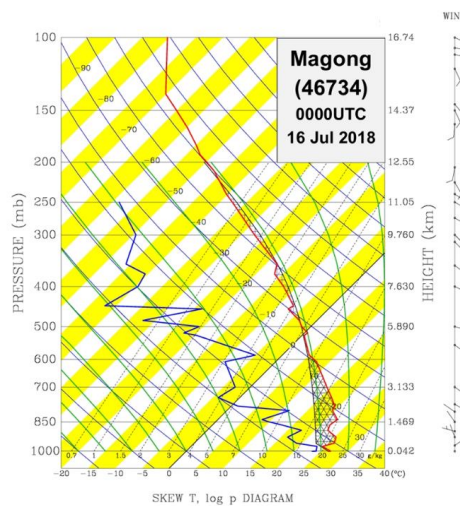


799

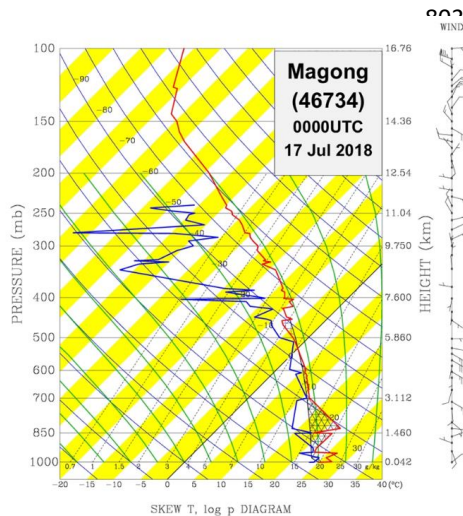
800 (a)



(b)



802 (c)



817

818

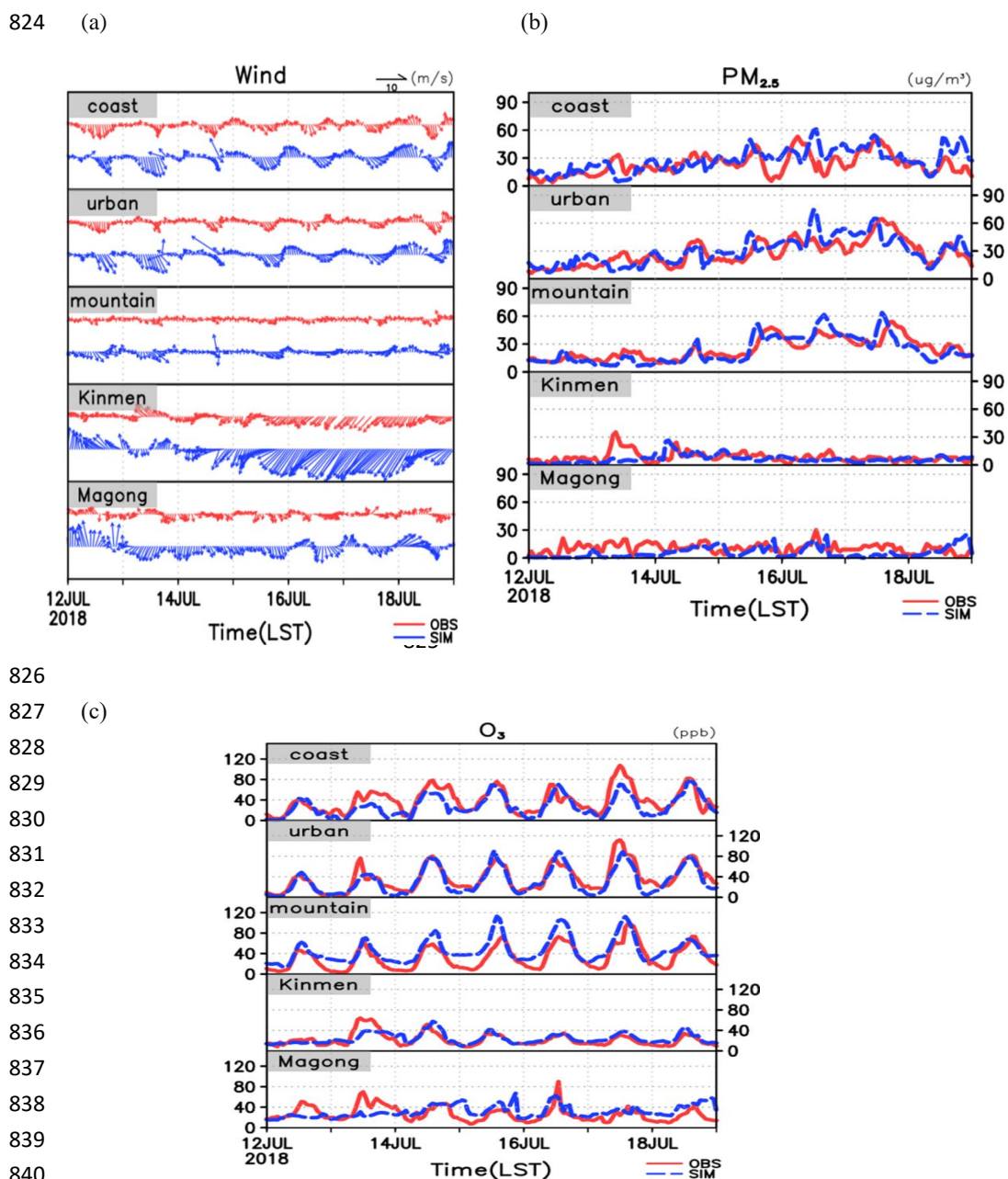
819

820

821 Fig. 4. Morning sounding launched at 00:00 UTC at station 46734 (located at MG in

822 Fig. 1a) (a) 15 July (b) 16 July, and (c) 17 July.

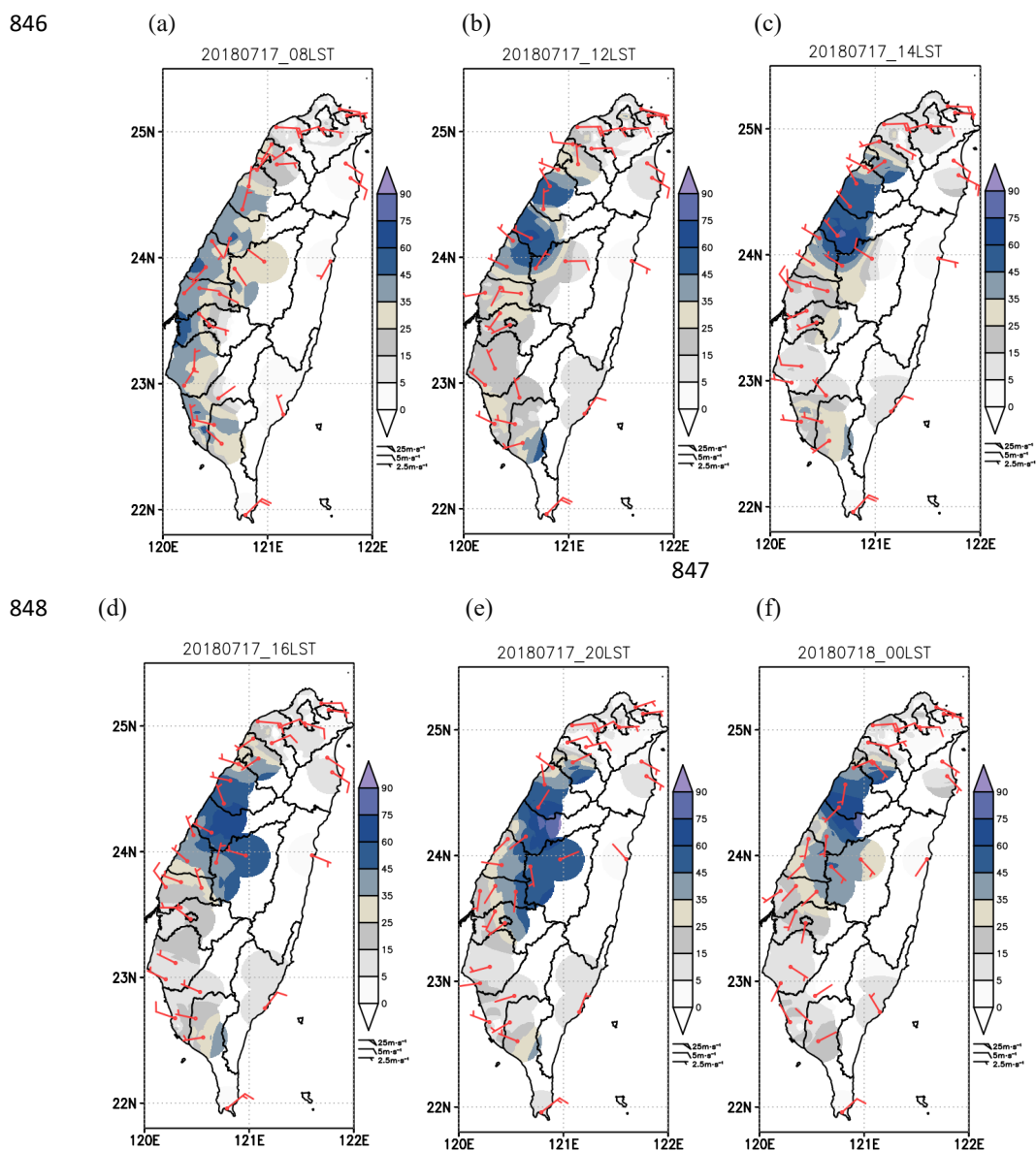
823



841 Fig. 5. Hourly variation of observed (red) and simulated (blue) values for (a) wind, (b)  
842 PM<sub>2.5</sub>, and (c) daytime (08:00-17:00LST) ozone between July 12 and 18, 2018, for  
843 the coastal, urban, and mountain stations as well as for the two island stations,  
844 Kinmen (KM) and Magong (MG).

845





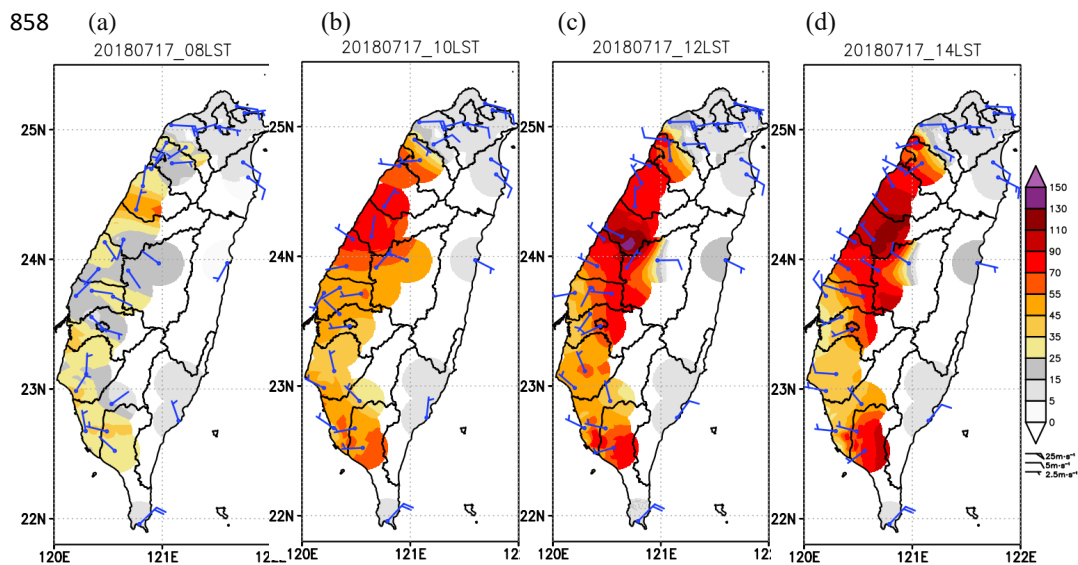
849  
850  
851  
852  
853  
854  
855  
856

Figure 6 Observed PM<sub>2.5</sub> concentration and wind recorded in Taiwan (a) at 08:00 LST (b) 12:00 LST (c) 14:00 LST (d) 16:00 LST (e) 20:00 LST, 17 July (f) 00:00 LST, 18 July, 2018.



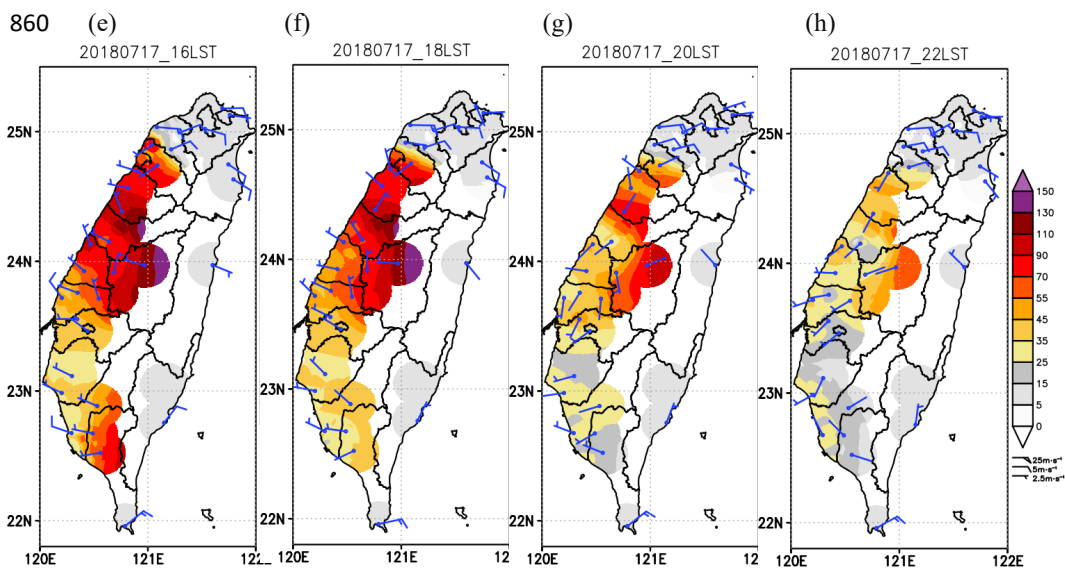
857

858



859

860



861

862

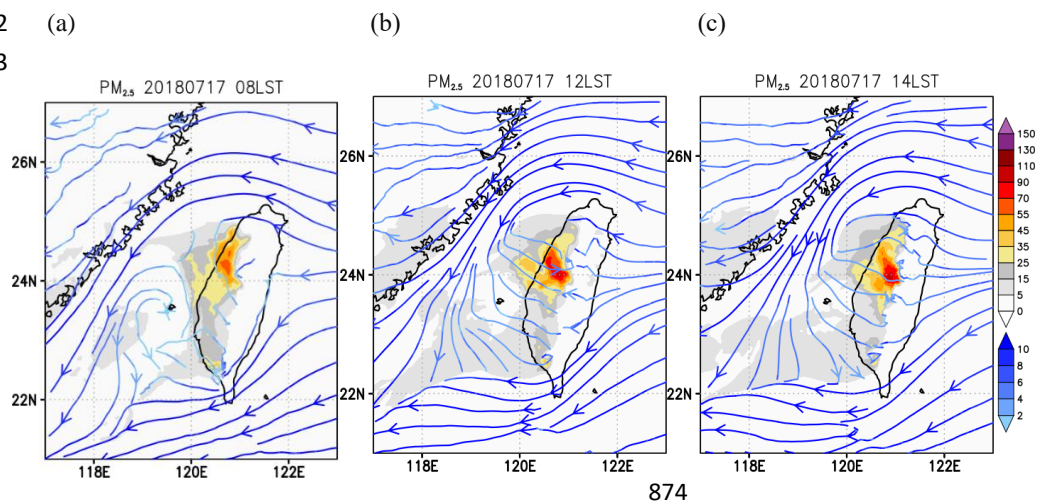
863

864

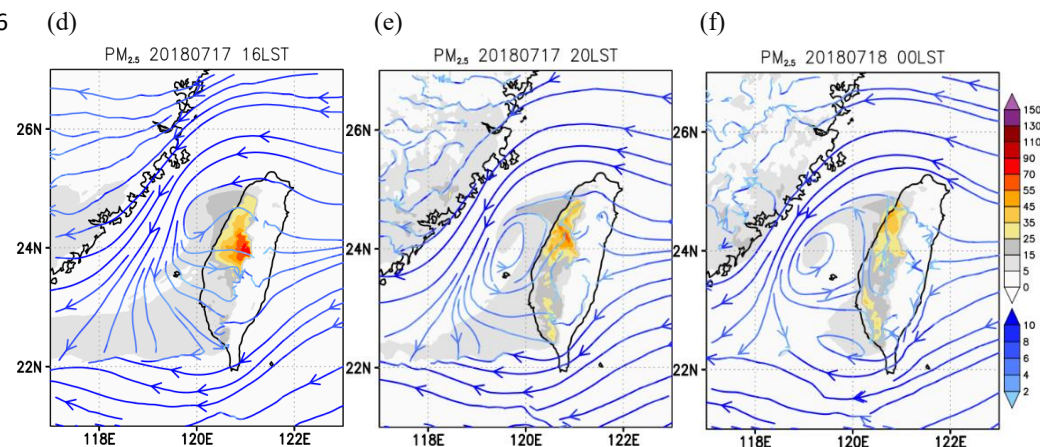
865 Figure 7 Observed ozone concentration (ppb) and wind recorded in Taiwan at (a)  
866 08:00 LST (b) 10:00 LST (c) 12:00 LST (d) 14:00 LST (e) 16:00 LST (f) 18:00 LST  
867 (g) 20:00 LST (h) 22:00 LST, 17 July, 2018.



868  
869  
870  
871  
872  
873

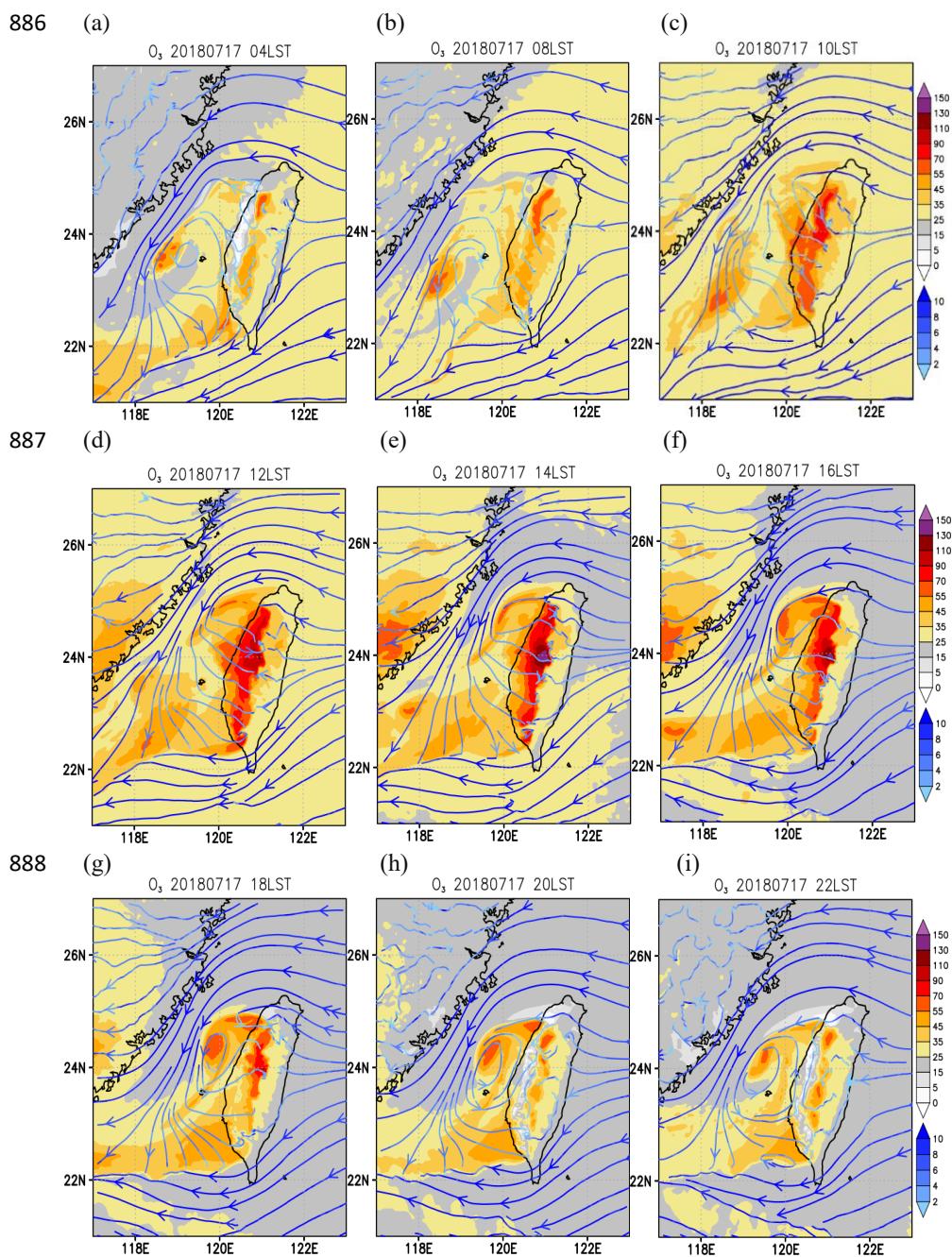


875  
876



877  
878  
879  
880  
881  
882  
883  
884  
885

Figure 8 Simulated streamline and PM<sub>2.5</sub> concentration ( $\mu\text{g}/\text{m}^3$ ) in Taiwan (a) at 08:00 LST (b) 12:00 LST (c) 14:00 LST (d) 16:00 LST (e) 20:00 LST, 17 July (f) 00:00 LST, 18 July, 2018.



889  
890 Figure 9 Simulated streamline and ozone concentration (ppb) in Taiwan at (a) 04:00  
891 LST (b)08:00LST (c) 10:00 LST (d) 12:00 LST (e) 14:00 LST (f) 16:00 LST,  
892 (g)18:00 (h) 20:00 LST, (i) 22:00 LST, 17 July, 2018 .

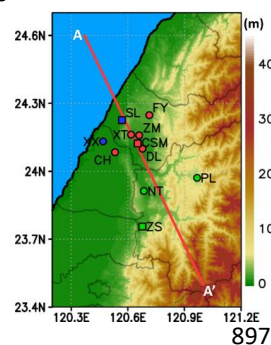


893

894

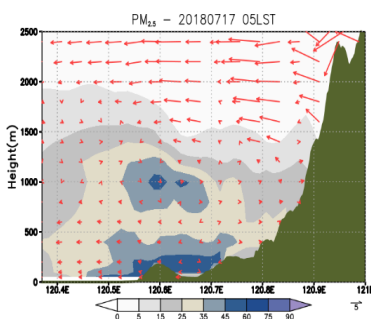
895 (a)

896

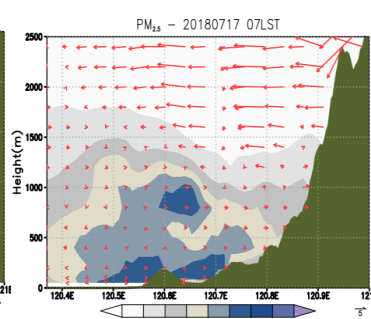


897

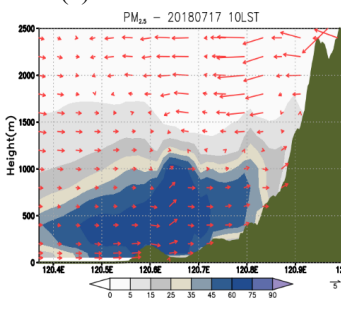
(b)



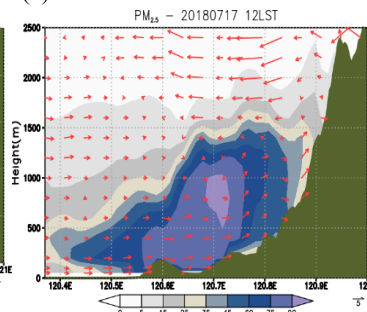
(c)



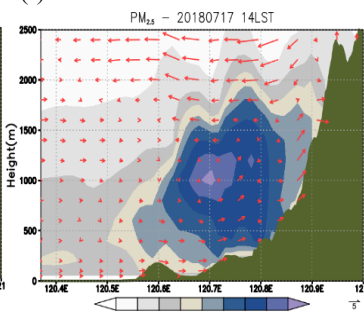
898 (d)



(e)

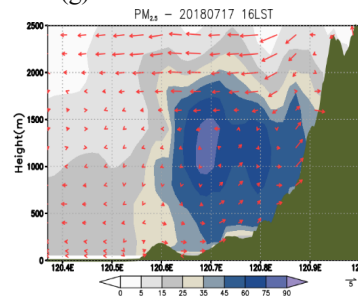


(f)

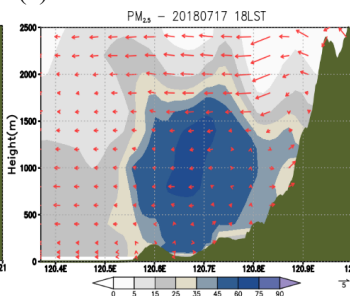


899

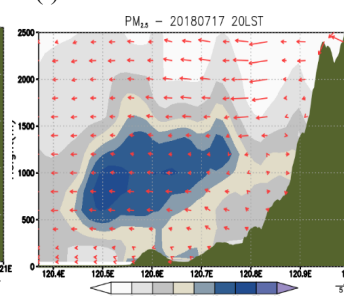
900 (g)



(h)



(i)



901

902

903 Figure 10 (a) The geographic location of study area in central Taiwan and the location

904 of NW-SE cross section AA'. Wind field distribution and PM<sub>2.5</sub> concentration (unit:

905 μg/m<sup>3</sup>) along the northwest–southeast cross section at (b) 05:00 LST (c) 07:00 LST

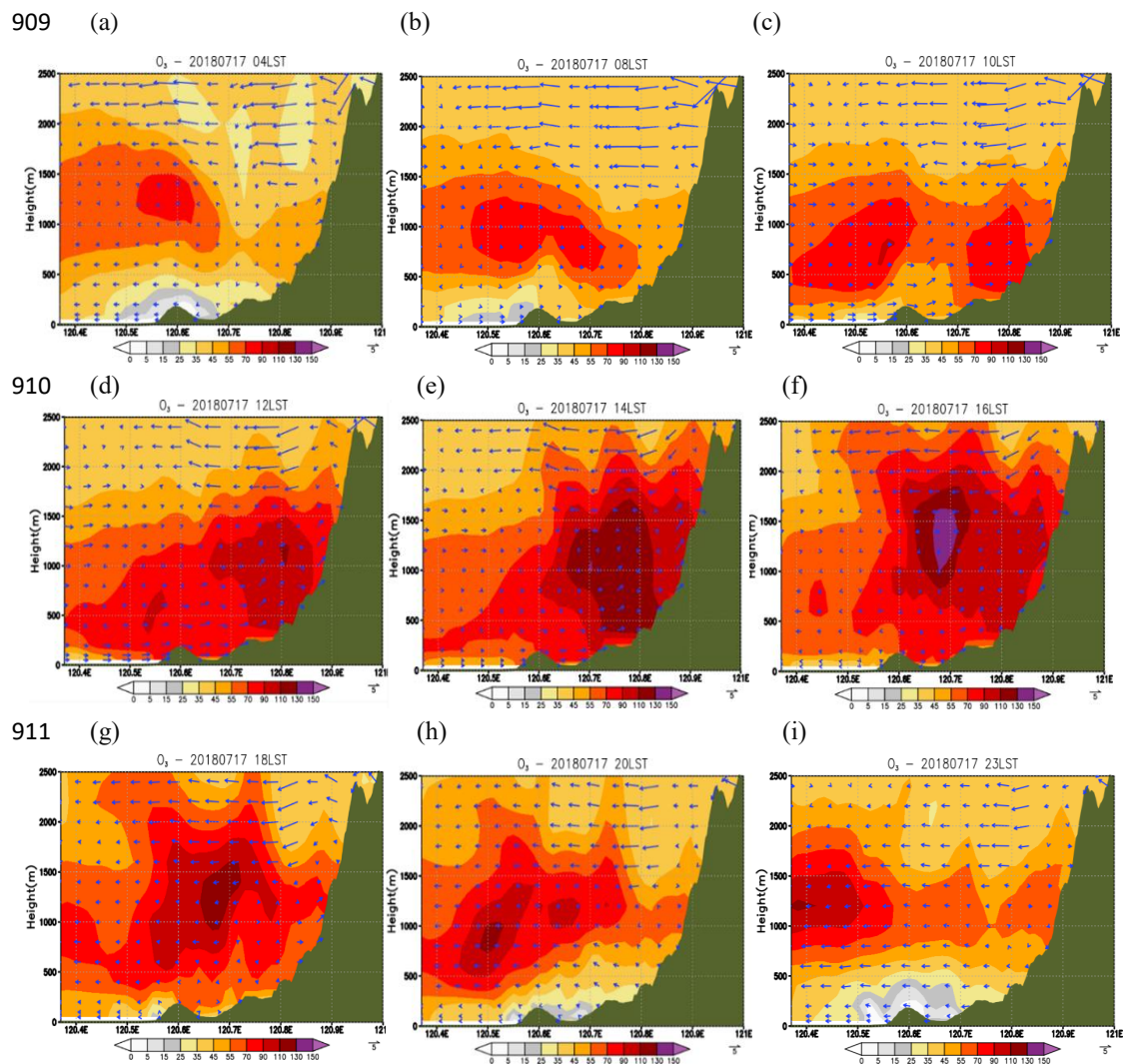
906 (d) 10:00 LST (e) 12:00 LST (f) 14:00 LST (g) 16:00 LST (h) 18:00 LST (i) 20:00

907 LST, 17 July, 2018.



908

909



910

911

912

913

914

915

916 Figure 11 Wind field distribution and ozone concentration (unit: ppb) along the

917 northwest–southeast cross section AA' in Figure 10a, at (a) 04:00 LST (b) 08:00

918 LST (c) 10:00 LST (d) 12:00 LST (e) 14:00 LST (f) 16:00 LST (g) 18:00 LST (h)

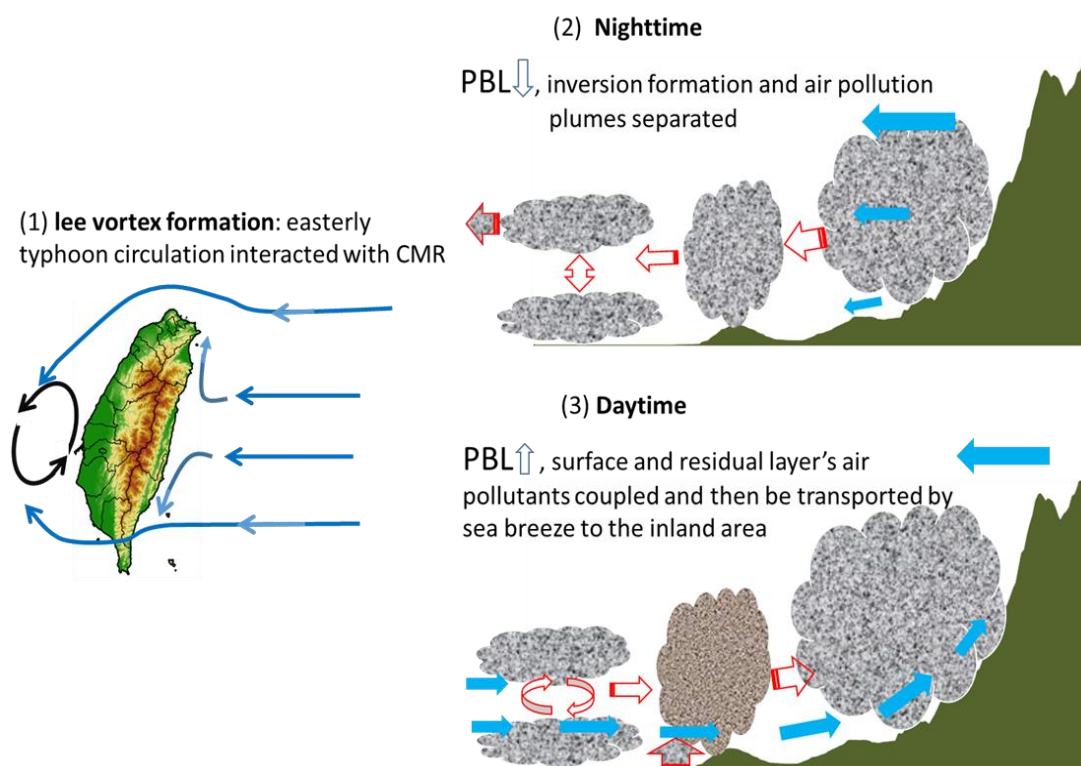
919 20:00 LST (i) 23:00 LST

920

921



922  
923  
924  
925



926  
927  
928  
929  
930  
931  
932  
933  
934  
935  
936  
937

Figure 12 Schematic of the processes of air quality deterioration episode associated with typhoon over Taiwan's western plain